[redacted]

Copy 91

RM A53G31

NACA RM A53G31

NACA

RESEARCH MEMORANDUM

A CORRELATION BY MEANS OF TRANSONIC SIMILARITY RULES OF THE EXPERIMENTALLY DETERMINED CHARACTERISTICS OF 18 CAMBERED WINGS OF RECTANGULAR PLAN FORM

By John B. McDevitt

Ames Aeronautical Laboratory
Moffett Field, Calif.

NATIONAL ADVISORY COMMITTEE
FOR AERONAUTICS

WASHINGTON

September 28, 1953

RM-A53G31

[redacted]

NATIONAL ADVISORY COMMITTEE FOR AERONAUTICS

RESEARCH MEMORANDUM

A CORRELATION BY MEANS OF TRANSONIC SIMILARITY RULES OF THE EXPERIMENTALLY DETERMINED CHARACTERISTICS OF 18 CAMBERED WINGS OF RECTANGULAR PLAN FORM

By John B. McDevitt

SUMMARY

The effects of one type of camber on the aerodynamic characteristics of rectangular wings have been studied by correlating the experimental data for a series of related wings by means of the transonic similarity rules. The experimental data were obtained by use of a transonic bump over a Mach number range from 0.60 to 1.10, with corresponding Reynolds numbers from 1.70 to 2.05 million. The wing models were rectangular in plan form; had NACA 63A2XX and 63A4XX sections; thickness-to-chord ratios of 0.04, 0.06, and 0.08; and aspect ratios of 1, 1.5, 2, 3, and 4. The results of a previously published correlation study for similar wings having symmetrical profiles, NACA 63A0XX sections, have been included in this report and are used as a basis for comparing the effects of changes in camber.

The results of this correlation study indicate that the subsonic and transonic characteristics of cambered, rectangular wings of moderate to low aspect ratio vary smoothly with changes in profile camber and camber-to-thickness ratio. By use of the transonic similarity rules the experimental data for a wide range of Mach numbers and wing geometric variables have been presented in the form of a few concise figures which correlate the subsonic and transonic characteristics of rectangular wings having NACA 63AXXX airfoils with $a = 0.8$ mean lines.

INTRODUCTION

The transonic bump of the Ames 16-foot high-speed wind tunnel has been used for a survey of the effects of aspect ratio, thickness, and camber for wings of rectangular plan form at high subsonic and transonic speeds.

The first part of this experimental survey covered a systematic variation of wing thickness and aspect ratio. The data for this portion of the survey have been published in reference 1 and an analysis, by application of the transonic similarity rules, has been published in reference 2. The next part of this survey was conducted to determine the effects of one type of camber on the transonic characteristics of rectangular wings. The data for the cambered-wing series are given in reference 3, and an analysis of some of these data will be made in this report.

As in reference 2, the present analysis will make extensive use of the transonic similarity rules, references 4 to 9. These rules of flow correspondence are particularly useful since they provide a unified method of data presentation which is applicable at all speeds.

NOTATION

A	aspect ratio, $\frac{b}{c}$
b	wing span
c	wing chord
C_D	total drag coefficient, $\frac{\text{total drag}}{qS}$
$C_{D_{int}}$	intercept drag coefficient for a linear variation of C_D with C_L^2 (See sketch (b).)
$(C_{D_P})_{int}$	intercept pressure-drag coefficient for a linear variation of C_D with C_L^2 (See sketch (b).)
ΔC_D	drag coefficient due to lift, $C_D - C_{D_{int}}$
C_L	lift coefficient, $\frac{\text{lift}}{qS}$
$C_{L_{opt}}$	optimum lift coefficient (lift coefficient for maximum lift-drag ratio)
C_m	pitching-moment coefficient, referred to 0.25 c, $\frac{\text{pitching moment}}{qSc}$
C_p	pressure coefficient
h	camber, maximum displacement of profile mean line from chord line (See sketch (a).)
$\frac{h}{t}$	camber-to-thickness ratio

$\left(\frac{L}{D}\right)_{max}$	maximum lift-drag ratio
M	free-stream Mach number
q	dynamic pressure
S	wing area
$\frac{t}{c}$	thickness-to-chord ratio
α	angle of attack
α_o	angle of attack for zero lift
γ	ratio of specific heats (for air $\gamma = 1.4$)
$\left(\frac{x}{c}\right)_{C.L.}$	center of lift, measured in percent of chord from the wing leading edge (See eqs. (17) and (18).)
τ	ordinate-amplitude parameter
$\frac{dC_L}{d\alpha}$, C_{L_α}	slope of lift curve
$\frac{dC_m}{dC_L}$	slope of pitching-moment curve

TEST PROCEDURE AND DESCRIPTION OF MODELS

The experimental data for the symmetrical wings (ref. 1) and for the cambered wings (ref. 3) were obtained by identical testing procedures. The semispan wing models were mounted in the high-velocity field of a bump in the Ames 16-foot high-speed wind tunnel. The streamlines of the flow over the bump were slightly curved, and there were Mach number gradients in the plane of the wing. Typical Mach number contours are presented in references 1 and 3. The gradients were most pronounced at the higher Mach numbers and had the greatest effect for the larger aspect ratios. The precise effects of the nonuniformity of the flow field are, in general, unknown, but some rounding off of any sharp breaks in the force and moment variation with Mach number can be expected.

The wings tested were rectangular in plan form with NACA 63A-series sections (figs. 1 and 2). The cambered wings had NACA 63A2XX and 63A4XX sections with an $a = 0.8$ (modified) mean line. (A discussion of this modified mean line is given in ref. 10.) The cambered-wing data were obtained for a Mach number range from 0.60 to 1.10, which corresponded

to a Reynolds number range from 1.70 to 2.05 million. A more complete description of the wing models and the testing procedure is given in references 1 and 3.

DATA CORRELATION

The data correlation will be made according to the same simplified form of the transonic similarity rule as used in reference 2,

$$\frac{C_p}{\tau^{2/3}} = P\left[\frac{M^2-1}{(t/c)^{2/3}}, A\left(\frac{t}{c}\right)^{1/3}, \frac{\alpha}{t/c}, \frac{h}{t}; \frac{x}{c}, \frac{y}{b}\right] \tag{1}$$

where the ordinate-amplitude parameter τ may be replaced by α, t/c, or h/c, as best suits the particular problem at hand. The variations between Mach number, aspect ratio, and thickness ratio implied by the constancy of the two similarity parameters $(M^2-1)/(t/c)^{2/3}$ and $A(t/c)^{1/3}$ are shown in figure 3.

In order that the transonic similarity rules can be used in the data analysis, the wings have been grouped into families according to the value of the camber-to-thickness ratio h/t. The camber parameter h represents the amount of camber and is defined as the maximum displacement of the mean line from the chord line (see sketch (a)).

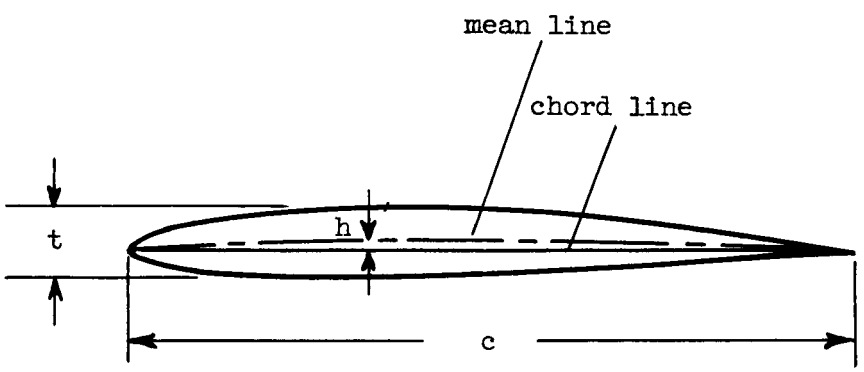

Sketch (a).- Wing-profile nomenclature.

Not all the cambered wings tested (ref. 3) have been used for the correlation study of this report. Profiles having h/t ratios greater than 0.5, for which the lower surfaces are concave along a major portion of the chord, were excluded from consideration. Also excluded from consideration were those wings having thickness-to-chord ratios of 0.02 and 0.10 since it was known from the previous correlation study of the

symmetrical wings (ref. 2) that these thicknesses do not fit well into the correlation scheme. For very thin wings the boundary layer is known to constitute an appreciable part of the effective wing thickness, while for wings of large thickness the simplified potential equation from which the similarity rules are obtained is apparently not adequate.

The cambered wings chosen for the data correlation have been grouped into three families for which the camber-to-thickness ratios h/t are 0.222, 0.333, and 0.444. These airfoils are listed in the following table:

h/t	NACA profile	t/c	h/c	Aspect ratios
0.222	63A206	0.06	0.0133	4, 3, 2, 1.5, 1
.333	63A204	.04	.0133	4, 3, 2, 1.5, 1
	63A408	.08	.0266	4, 2, 1
.444	63A406	.06	.0266	4, 3, 2, 1.5, 1

The results of the symmetrical-wing correlation ($h/t = 0$) in reference 2 are also presented in this report and are used as a basis for determining the effects of this type of camber on the transonic characteristics of rectangular wings.

Lift

The lift correlation is presented as separate studies of the lift-curve slope and of the displacement of the lift curve due to the presence of camber. For the wings considered in this report, the variation of lift coefficient with angle of attack is essentially linear at moderate angles of attack throughout the Mach number range, hence, it is convenient to assume a linear variation of C_L with α and to use in the data correlation the following generalized expression for lift-curve slope (see ref. 2):

$$\left.\begin{aligned}\left(\frac{t}{c}\right)^{1/3}\frac{dC_L}{d\alpha} &= L_1\left[\frac{M^2-1}{(t/c)^{2/3}}, A\left(\frac{t}{c}\right)^{1/3}, \frac{h}{t}\right]\\ C_L &\sim \alpha\end{aligned}\right\} \qquad (2)$$

C[redacted]

The displacement of the lift curve can be studied by use of either the generalized expression for the angle of attack for zero lift

$$\frac{\alpha_0}{h/c} = L_2\left[\frac{M^2-1}{(t/c)^{2/3}},\ A\left(\frac{t}{c}\right)^{1/3},\ \frac{h}{t}\right] \tag{3}$$

or the generalized expression for the lift coefficient at zero angle of attack

$$\left(\frac{t}{c}\right)^{1/3}\frac{(C_L)_{\alpha=0}}{h/c} = L_3\left[\frac{M^2-1}{(t/c)^{2/3}},\ A\left(\frac{t}{c}\right)^{1/3},\ \frac{h}{t}\right] \tag{4}$$

Angle of attack for zero lift.- The variation of the angle of attack for zero lift, α_0, with Mach number is presented in figure 4, and the correlation of these data for constant values of $(M^2-1)/(t/c)^{2/3}$ is presented in figure 5. It should be recognized that the angle of attack for zero lift is particularly sensitive to model construction details, tunnel flow characteristics and the accuracy of measurements, making this a difficult parameter to correlate.

Since the parameter $\alpha_0/(h/c)$ did not show a systematic dependence on the value of the camber-to-thickness ratio h/t, all the wings of the various camber-to-thickness families have been grouped together in the correlation and a single curve has been drawn through the data points. The correlation is cross-plotted for constant values of $A(t/c)^{1/3}$ in figure 6.

For Mach numbers less than the critical (which occurs in the neighborhood of $(M^2-1)/(t/c)^{2/3} = -2$) the angle of attack for zero lift shows little change with changes in Mach number, and the experimental values of α_0 for wings of large aspect ratio are closely predicted by two-dimensional flow theory.[1] When the critical Mach number is exceeded, the changes occurring with increasing Mach number are sudden and quite large for all but the very low aspect ratios which are characteristically insensitive to changes in the Mach number.

Lift-curve slope.- The variation of the lift-curve slope, evaluated at $\alpha = 0$, with Mach number is presented in figure 7, and the correlation of the generalized lift-curve slope $(t/c)^{1/3}\,(dC_L/d\alpha)_{\alpha=0}$ for constant $(M^2-1)/(t/c)^{2/3}$ is presented in figure 8. The correlation is presented separately for each camber-to-thickness family since the lift-curve slope appeared to depend on the camber-to-thickness ratio at transonic speeds for wings of large aspect ratio.

[1]The theoretical value shown in figures 4, 5, and 6 was calculated by use of the a = 0.8 (modified) mean-line data of figure 3, reference 10, and equation (16) of reference 11.

In figure 8 the experimental data for subsonic speeds are compared with the Weissinger lifting-line theory (ref. 12), and at supersonic speeds a comparison is made with slender-wing theory (refs. 13 and 14). At $M = 1$ both theories give the same result

$$C_L = \frac{\pi}{2} A\alpha \tag{5}$$

or, in the similarity scheme,

$$\left(\frac{t}{c}\right)^{1/3} \frac{dC_L}{d\alpha} = \frac{\pi}{2} A \left(\frac{t}{c}\right)^{1/3} \tag{6}$$

At $M = 1$ the experimental data for the symmetrical profiles are in good agreement with equation (6) for values of $A(t/c)^{1/3}$ less than about 1, and for the cambered profiles the agreement extends over a considerably larger range of $A(t/c)^{1/3}$ values.

The correlation is cross-plotted in figure 9 for constant values of h/t and $A(t/c)^{1/3}$. Camber has no appreciable effect on the lift-curve slope at subcritical speeds nor for the wings of low aspect ratio ($A(t/c)^{1/3}$ less than about 1) at transonic speeds. For wings of larger aspect ratio at transonic speeds the lift-curve slope appeared to increase with increasing h/t.

Drag

Whenever possible it is convenient to separate the drag coefficient into components of friction drag, minimum pressure drag, and drag due to lift,

$$C_D = C_{D_f} + (C_{D_p})_{min} + \Delta C_D \tag{7}$$

For wings having symmetrical profiles it is often assumed that the friction drag at transonic speeds can be approximated by the minimum drag at some subcritical Mach number, say at 0.7. The friction drag, however, cannot be correlated by application of the transonic similarity rules.

When the wing is cambered it is difficult to separate the drag into components according to equation (7); in particular, it is difficult to obtain a minimum pressure drag which is free from induced drag effects. A drag analysis of cambered-wing data is complicated further by the large changes in viscous effects which may occur as the lift changes from positive to negative. These viscous effects must be separated from the pressure drag if the transonic similarity rule is to be applied. One way, which is based on a number of approximations, to separate the viscous effects from the pressure drag is the following:

Linear variations of C_D with C_L^2 and C_L with α are assumed and the drag data at very small lift coefficients and at lift coefficients greater than the optimum are ignored. The drag components are then defined according to the following sketch:

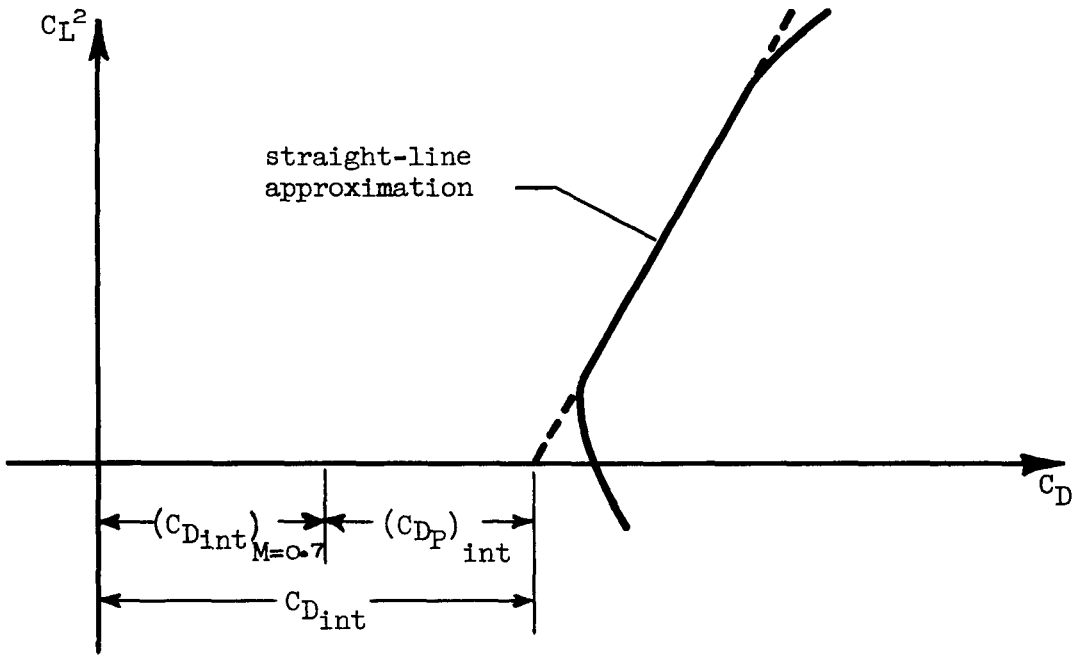

Sketch (b).- Drag nomenclature.

A straight line is drawn as far as possible through the C_D vs C_L^2 data points and the intercept of this straight line with the zero-lift axis is then used to define an intercept drag coefficient $C_{D_{int}}$. The intercept pressure drag is defined as

$$(C_{D_P})_{int} = C_{D_{int}} - (C_{D_{int}})_{M = 0.7} \tag{8}$$

and the slope of the straight-line approximation $\Delta C_D/C_L^2$ will be used in the data correlation as a measure of the drag due to lift.

The intercept drag coefficient $C_{D_{int}}$, as defined here, is a fictitious minimum-drag coefficient and the actual minimum-drag coefficient is somewhat higher. However, this method of analysis has been found to give a good correlation of the experimental data, except in the vicinity of the critical Mach number, when the similarity parameters are used. A comparison of the cambered-wing data with the symmetrical-wing data has indicated a smooth dependence of the intercept pressure drag and the drag due to lift on the value of the camber-to-thickness ratio h/t.

The experimental drag data for the cambered wings being studied in this report are presented in figure 10 in the form C_D versus C_L^2.

The straight-line approximations extend in all cases at least up to the lift coefficient for $(L/D)_{max}$. The variation of $C_{D_{int}}$ with Mach number for these wings is presented in figure 11.

Intercept drag at 0.7 Mach number.- Before the correlation of the intercept pressure drag can be made, it is necessary to evaluate the subcritical intercept drag (at 0.7 Mach number) for use in equation (8). The variation of $(C_{D_{int}})_{M = 0.7}$ with camber ratio is shown in figure 12. (The subcritical intercept drag for cambered wings may be thought of as corresponding to the friction drag of symmetrical wings.)

Intercept pressure drag.- The intercept pressure drag, equation (8), can be correlated by use of the similarity rule

$$\frac{(C_{D_P})_{int}}{(t/c)^{5/3}} = D\left[\frac{M^2-1}{(t/c)^{2/3}}, A\left(\frac{t}{c}\right)^{1/3}, \frac{h}{t}\right] \tag{9}$$

The correlation is presented in figure 13 and compared with the results of the symmetrical-wing-data correlation (dashed lines) of reference 2. The transonic similarity rule, at least in the simplified form used here, does not correlate accurately the initial (subsonic) drag rise but the correlation is good near $M = 1$ where the drag rise is greatest.[2]

The correlation indicates that the intercept pressure drag increased smoothly with increasing camber-to-thickness ratio. For moderate aspect

[2]In the literature concerning transonic flow theory various forms of the similarity rules have been given (refs. 4 to 9). All are equivalent at a Mach number of 1 but differ slightly at the nonsonic Mach numbers according to the assumptions made in obtaining the fundamental equations. A form of the similarity rule which can be expected to give a better correlation of experimental data in the vicinity of the critical Mach number is (ref. 4)

$$\frac{[(\gamma+1)M^2]^{1/3}}{\tau^{2/3}} C_p = P\left\{\frac{M^2-1}{[(\gamma+1)M^2\ t/c]^{2/3}}, A\left[(\gamma+1)M^2\frac{t}{c}\right]^{1/3}, \frac{\alpha}{t/c}, \frac{h}{t}\right\}$$

$$\tau \sim \frac{t}{c}, \frac{h}{c}, \alpha$$

The simplified form used in this report, (eq. (1)) has certain advantages, however, not only because of the relative simplicity of the invariants but because the particular invariant $A(t/c)^{1/3}$ contains only geometric parameters.

[redacted]

ratios the increase in drag coefficient is roughly proportional to the camber ratio squared. As the aspect ratio becomes very small, the camber effect tends to disappear, while for very large aspect ratios the generalized coefficients $(C_{D_P})_{int}/(t/c)^{5/3}$ apparently approach constant values which increase with increasing h/t. Data, however, were not available for sufficiently large aspect ratios to assess accurately the camber effect for two-dimensional flow.

This correlation is cross-plotted in figure 14 for constant values of $A(t/c)^{1/3}$ and h/t. The region of poor correlation at the start of the drag rise is indicated by dashed lines. When the wings were symmetrical in profile, the drag rise started at very nearly the same value of the speed parameter $(M^2-1)/(t/c)^{2/3}$, that is, a decrease in the aspect ratio caused only a slight delay in the start of the drag rise. However, for increased camber-to-thickness ratio the drag rise started at a much lower Mach number and the aspect-ratio effect was pronounced.

Drag due to lift.- The drag-due-to-lift parameter $\Delta C_D/C_L^2$ is evaluated from the slopes of the straight-line approximations (solid lines) of the C_D vs C_L^2 curves of figure 10. The variation of $\Delta C_D/C_L^2$ with Mach number is shown in figure 15, and these data have been correlated in figure 16 according to the similarity rule

$$\left.\begin{aligned} \left(\frac{t}{c}\right)^{-1/3} \frac{\Delta C_D}{C_L^2} &= \Delta D \left[\frac{M^2-1}{(t/c)^{2/3}},\ A\left(\frac{t}{c}\right)^{1/3},\ \frac{h}{t}\right] \\ C_L &\sim \alpha \\ \Delta C_D &\sim C_L^2 \end{aligned}\right\} \tag{10}$$

and the results of this correlation are cross-plotted in figure 17.

The dashed lines in figure 16 represent the limits for drag with full leading-edge suction and drag with no leading-edge suction. The theoretical drag due to lift with full leading-edge suction is (when an elliptical spanwise variation of loading is assumed)

$$\Delta C_D = \frac{C_L^2}{\pi A} \tag{11}$$

and for no leading-edge suction the following approximate relationship can be used:

$$\Delta C_D = C_L \alpha \tag{12}$$

In terms of the similarity parameters these equations become

$$\left(\frac{t}{c}\right)^{-1/3} \frac{\Delta C_D}{C_L^2} = \frac{1}{\pi A (t/c)^{1/3}} \tag{13}$$

$$\left(\frac{t}{c}\right)^{-1/3} \frac{\Delta C_D}{C_L^2} = \frac{1}{(t/c)^{1/3}\, dC_L/d\alpha} \tag{14}$$

Numerical values for $(t/c)^{1/3} C_{L_\alpha}$ are presented in figure 9.

The concept of a leading-edge force is not easily adapted to a discussion of experimental data because of the many factors involved. In addition to the changes in flow separation and in the boundary-layer development with changing angle of attack, there are other factors such as the interaction of shock waves with the boundary layer that lead to departures of the drag polars from the parabolic shape. However, equations (13) and (14) are helpful in evaluating the effects of changes in Mach number, aspect ratio, thickness ratio, and camber ratio.

As evidenced by the correlation shown in figure 16, the drag due to lift seems to decrease consistently with increasing camber-to-thickness ratio throughout the entire Mach number range for the wings of moderate to low aspect ratio ($A(t/c)^{1/3}$ less than about 1.5).

Moment

The pitching-moment characteristics are analyzed in two parts: the evaluation of pitching moment at zero angle of attack, or at zero lift, and the variation of pitching moment with angle of attack.

Pitching moment for zero angle of attack.- The variation of pitching-moment coefficient with Mach number for zero angle of attack is shown in figure 18. The correlation of this data according to the similarity rule

$$\frac{(t/c)^{1/3}}{h/c} (C_m)_{\alpha=0} = M_o \left[\frac{M^2-1}{(t/c)^{2/3}},\ A\left(\frac{t}{c}\right)^{1/3},\ \frac{h}{t} \right] \tag{15}$$

is presented in figure 19 and the results are cross-plotted for constant values of $A(t/c)^{1/3}$ in figure 20.

Throughout the correlation the generalized parameter $\frac{(t/c)^{1/3}}{h/c}(C_m)_{\alpha=0}$ is essentially independent of the camber-to-thickness ratio h/t. Therefore, the zero-angle-of-attack moment $(C_m)_{\alpha=0}$ can be considered to be linearly proportional to the camber ratio h/c throughout the speed range. The variation of $(C_m)_{\alpha=0}$ with changes in aspect ratio and Mach number is pronounced, in particular, the wings of large aspect ratio undergo large moment changes on entering the transonic speed range.

Pitching moment for zero lift.- The pitching moment for zero lift is considered to be a couple. The correlation of the data for the generalized pitching-moment coefficient is presented in figures 21 and 22. The results here are essentially the same as those discussed in the previous section.

Pitching-moment-curve slope.- The moment-curve slope is expressed symbolically in the similarity scheme as

$$\frac{dC_m}{dC_L} = M\left[\frac{M^2-1}{(t/c)^{2/3}}, A\left(\frac{t}{c}\right)^{1/3}, \frac{\alpha}{t/c}, \frac{h}{t}\right] \tag{16}$$

Because the variation of pitching moment with lift is nonlinear except for wings of large aspect ratio, the following correlation has been made for several constant values of $\alpha/(t/c)$.

The variation of dC_m/dC_L with Mach number for $\alpha/(t/c) = 0$ is presented in figure 23 and the corresponding correlation in figure 24. Curves for constant $A(t/c)^{1/3}$ are shown in figure 25 for $\alpha/(t/c) = 0$ and for $\alpha/(t/c) = 1$ and 2.

The effects of Mach number on the moment-curve slope are pronounced for these wings of rectangular plan form, except, of course, those wings of very low aspect ratio which are relatively insensitive to Mach number changes. For all wings except those of very low aspect ratio, dC_m/dC_L changed from a slightly positive value at subcritical speeds to a large negative value at transonic speeds.

Center-of-lift travel.- The trim changes associated with flight into the transonic speed range depend on changes in the zero-lift moment and on changes in the additional moment that occur for finite lift. The changes in the zero-lift moment have been discussed previously. The trim changes occurring at finite lift are most easily evaluated by studying the position of the wing center of lift at various speeds.

The center of lift is defined by the equation

$$\left(\frac{x}{c}\right)_{C.L.} = 0.25 - \frac{\Delta C_m}{C_L} \tag{17}$$

The moment is referred to the quarter point of the chord, the center of lift is measured from the wing leading edge and given in percent of chord, and the moment due to lift is defined as

$$\Delta C_m = C_m - (C_m)_{C_L = o} \tag{18}$$

Cross plots indicating the center-of-lift travel are presented in figure 26. The center of lift is shown to move progressively toward the leading edge as the aspect ratio goes to zero. This is in agreement with the various low-aspect-ratio theories which find the center of pressure located at the leading edge for rectangular plan forms. When the aspect ratio is large (greater than about 3) the center of lift is near the quarter point of the chord at subcritical speeds but moves rapidly rearward toward midchord at transonic speeds. By increasing the camber-to-thickness ratio h/t, this rearward movement of the center of lift at supercritical speeds is increased further.

Maximum Lift-Drag Ratio and Optimum Lift Coefficient

Maximum lift-drag ratio.- The variation of the maximum lift-drag ratio with Mach number is shown in figure 27 for the symmetrical and cambered wings having aspect ratios from 1 to 4. Some understanding of the variations of $(L/D)_{max}$ with changes in aspect ratio, thickness ratio, and camber ratio can be obtained by the help of the equation

$$\left(\frac{L}{D}\right)_{max} = \frac{1}{2\sqrt{\left[C_{D_f} + (C_{D_P})_{min}\right]\frac{\Delta C_D}{C_L^2}}} \tag{19}$$

where it has been assumed that ΔC_D varies linearly with C_L^2. In terms of the transonic similarity parameters and the quantities introduced in sketch (b), this equation becomes

$$\left(\frac{L}{D}\right)_{max} = \frac{1}{2\frac{t}{c}\sqrt{\left[\frac{(C_{D_{int}})_{M=0.7}}{(t/c)^{5/3}} + \frac{(C_{D_P})_{int}}{(t/c)^{5/3}}\right]\left(\frac{t}{c}\right)^{-1/3}\frac{\Delta C_D}{C_L^2}}} \quad (20)$$

Because the subcritical intercept drag cannot be taken into the similarity scheme, a generalized expression for $(L/D)_{max}$ cannot be obtained. However, the results of previous correlations for intercept pressure drag and drag due to lift can be used to obtain an indication of the expected variations of $(L/D)_{max}$ for changes in aspect ratio, thickness ratio, and camber ratio. The following discussion is restricted to near-sonic values of the Mach number.

The correlation for the symmetrical wings (ref. 2) at near-sonic Mach numbers shows that for decreasing aspect ratios, the drag-due-to-lift parameter $(t/c)^{-1/3}(\Delta C_D/C_L^2)$ increases in nearly the same manner as the minimum pressure-drag parameter $(C_{D_P})_{min}/(t/c)^{5/3}$ decreases so that the maximum lift-drag ratio is relatively insensitive to aspect-ratio changes but tends toward an inverse variation with the thickness ratio (see eq. (20)).

An inspection of the data for the cambered-wing correlation in this report at near-sonic speeds shows that for increasing camber-to-thickness ratio, the drag due to lift decreases while the intercept pressure drag increases. Because of the opposite effect of these two variations, it could be expected that $(L/D)_{max}$ would not change greatly with changes in h/t.

Although the similarity rule does not apply, it is instructive to present the maximum lift-drag data in terms of the camber-to-thickness ratio h/t. This has been done in figure 28 for the sonic value of the free-stream Mach number. For wings of moderately low aspect ratio (aspect ratios from about 1 to about 3), the effect of adding a small amount of camber is to increase slightly the maximum lift-drag ratio. It is difficult to say what value of h/t is optimum but, apparently (excluding the very thin wing, $t/c = 0.02$, for which the boundary layer is a significant part of the wing effective thickness), the optimum occurs near $h/t = 0.25$ with the most beneficial effect for aspect ratios near 2.

Optimum lift coefficient.- The variation of the optimum lift coefficient, C_L for $(L/D)_{max}$, with Mach number is shown in figure 29. If a linear variation of ΔC_D with C_L^2 is assumed, the optimum lift coefficient is given by

$$C_{L_{opt}} = \sqrt{\frac{C_{D_f} + (C_{D_P})_{min}}{\Delta C_D / C_L^2}} \tag{21}$$

or, in terms of the similarity parameters and the drag nomemclature of sketch (b),

$$C_{L_{opt}} = \left(\frac{t}{c}\right)^{2/3} \sqrt{\frac{\frac{(C_{D_{int}})_{M=0.7}}{(t/c)^{5/3}} + \frac{(C_{D_P})_{int}}{(t/c)^{5/3}}}{(t/c)^{-1/3} \frac{\Delta C_D}{C_L^2}}} \tag{22}$$

By inspection of equation (22) it is readily seen that by increasing any of the parameters, aspect ratio, thickness ratio, or camber-to-thickness ratio, an increase in $C_{L_{opt}}$ can be expected. The experimental evidence indicates that the most pronounced changes occur at transonic speeds where the minimum drag changes are large.

CONCLUDING REMARKS

It was found that the camber effects at transonic speeds for rectangular plan forms can, in most cases, be correlated successfully with the help of the transonic similarity rules. By use of the transonic similarity rules the experimental data for a wide range of Mach numbers and wing geometric variables have been presented in the form of a few concise figures which correlate the subsonic and transonic characteristics of rectangular wings having NACA 63A-series sections with $a = 0.8$ mean lines.

Ames Aeronautical Laboratory
National Advisory Committee for Aeronautics
Moffett Field, Calif., July 31, 1953

REFERENCES

1. Nelson, Warren H., and McDevitt, John B.: The Transonic Characteristics of 17 Rectangular, Symmetrical Wing Models of Varying Aspect Ratio and Thickness. NACA RM A51A12, 1951.

2. McDevitt, John B.: A Correlation by Means of the Transonic Similarity Rules of the Experimentally Determined Characteristics of 22 Rectangular Wings of Symmetrical Profile. NACA RM A51L17b, 1952.

3. Nelson, Warren H., and Krumm, Walter J.: The Transonic Characteristics of 38 Cambered Rectangular Wings of Varying Aspect Ratio and Thickness as Determined by the Transonic-Bump Technique. NACA RM A52D11, 1952.

4. Busemann, Adolf: Application of Transonic Similarity. NACA TN 2687, 1952.

5. von Kármán, Theodore: The Similarity Law of Transonic Flow. Jour. Math. and Phys., vol. XXVI, no. 3, Oct. 1947, pp. 182-190.

6. Spreiter, John R.: Similarity Laws for Transonic Flow About Wings of Finite Span. NACA TN 2273, 1951.

7. Spreiter, John R.: On the Application of Transonic Similarity Rules. NACA TN 2726, 1952.

8. Berndt, Sune B.: Similarity Laws for Transonic Flow Around Wings of Finite Aspect Ratio. Kungl. Tekniska Högskolan. Tech. Note 14, Stockholm, Sweden, 1950.

9. Harder, Keith C.: Transonic Similarity Rules for Lifting Wings. NACA TN 2724, 1952.

10. Loftin, Laurence K., Jr.: Theoretical and Experimental Data for a Number of NACA 6A-Series Airfoil Sections. NACA Rep. 903, 1948.

11. Abbott, Ira H., von Doenhoff, Albert E., and Stivers, Louis S., Jr.: Summary of Airfoil Data. NACA Rep. 824, 1945.

12. DeYoung, John, and Harper, Charles W.: Theoretical Symmetric Span Loading at Subsonic Speeds for Wings Having Arbitrary Plan Form. NACA Rep. 921, 1950.

13. Jones, Robert T.: Properties of Low-Aspect-Ratio Pointed Wings at Speeds Below and Above the Speed of Sound. NACA Rep. 835, 1946. (Formerly NACA TN 1032)

14. Lomax, Harvard, and Sluder, Loma: Chordwise and Compressibility Corrections to Slender-Wing Theory. NACA TN 2295, 1951.

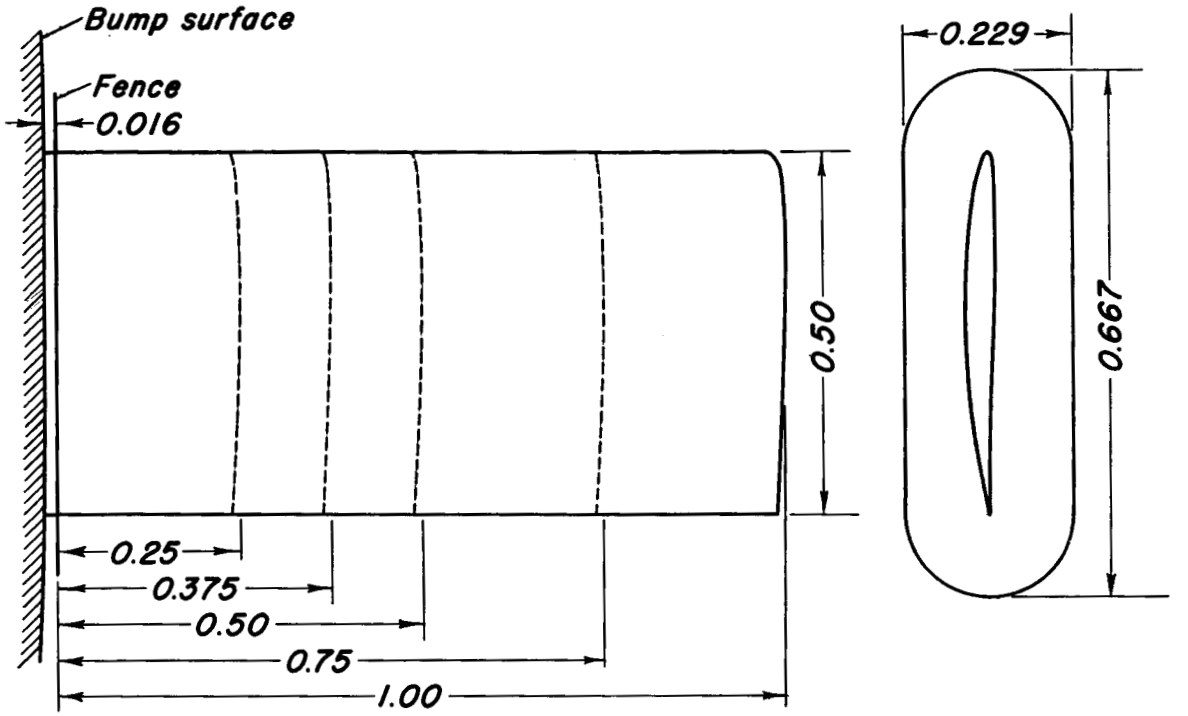

Aspect ratio	Semispan, feet	Area of semispan, square feet
1	0.25	0.125
1.5	.375	.1875
2	.50	.250
3	.75	.375
4	1.00	.500

Note:
All dimensions in feet.

Figure 1.–Dimensions and plan forms of the model.

NACA 63A206; $^{h}/_{t}$, 0.222

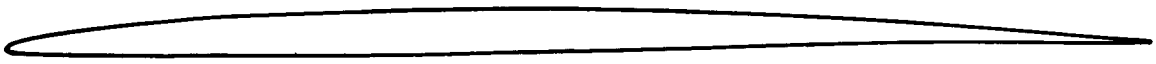

NACA 63A204; $^{h}/_{t}$, 0.333

NACA 63A408; $^{h}/_{t}$, 0.333

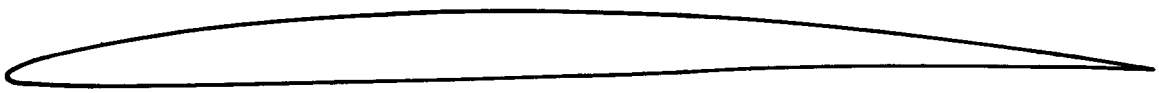

NACA 63A406; $^{h}/_{t}$, 0.444

Figure 2.–Profile of the wings.

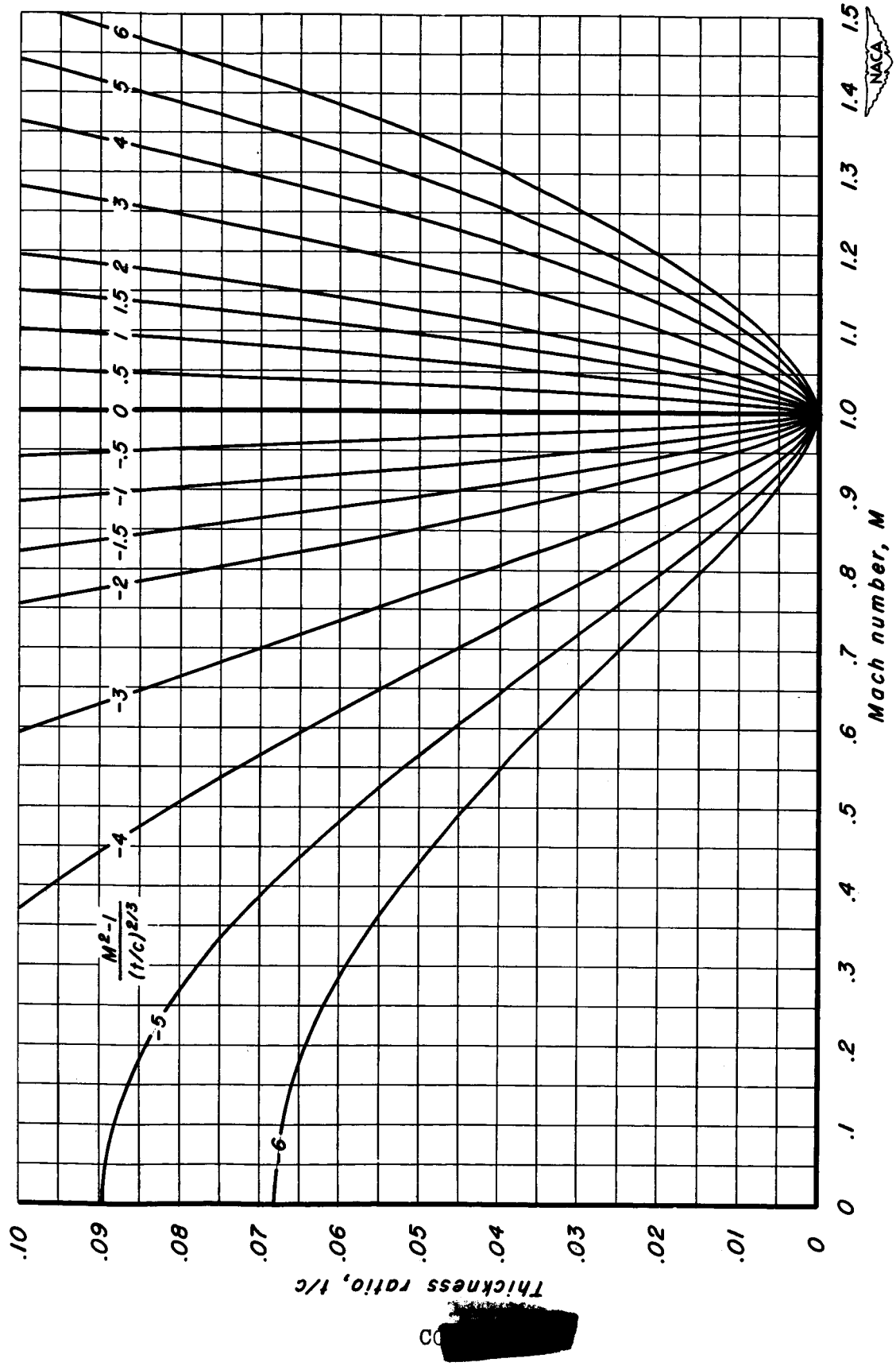

(a) Thickness ratio versus Mach number for constant $\frac{M^2-1}{(t/c)^{2/3}}$.

Figure 3.- The transonic similarity parameters.

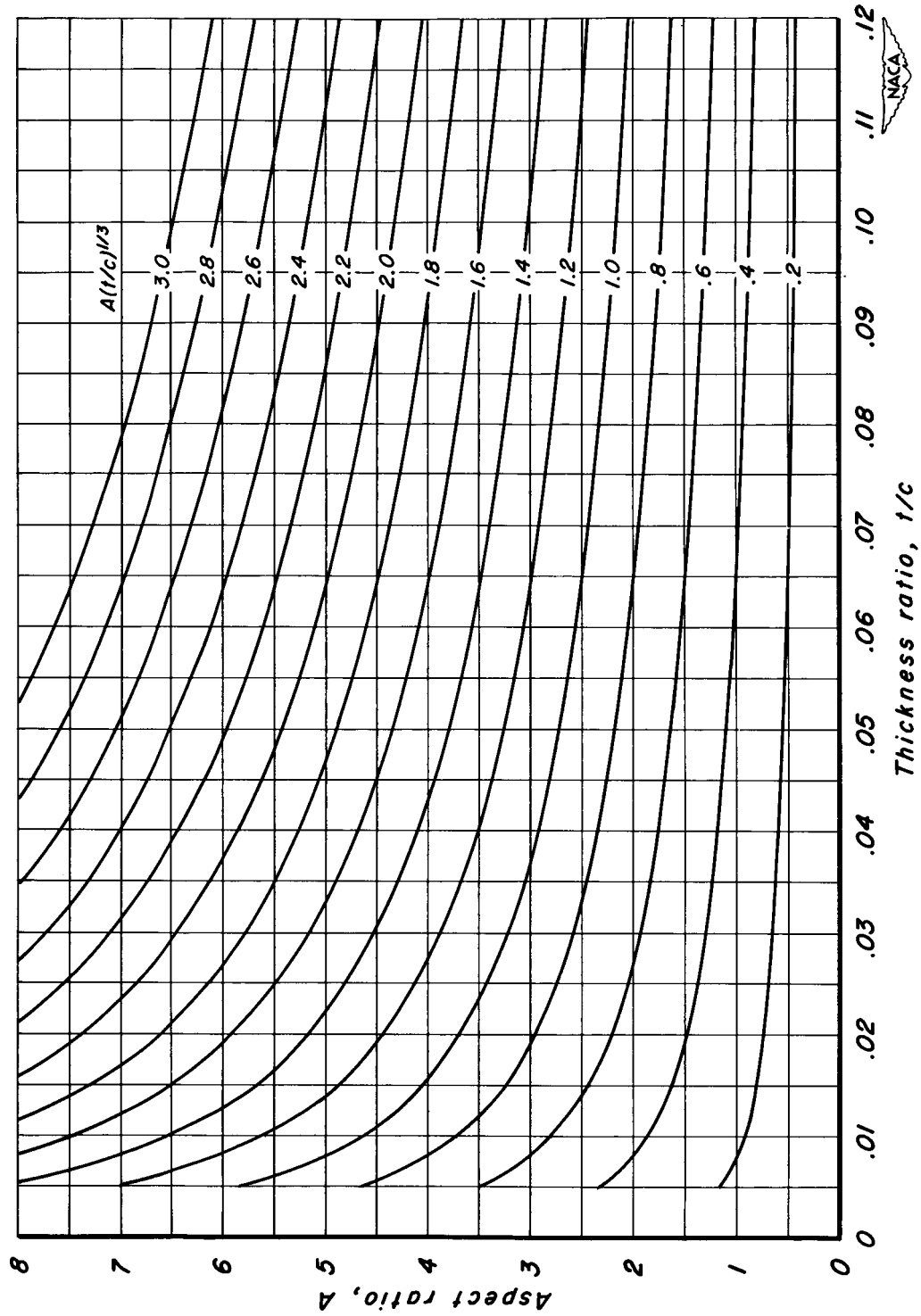

(b) Aspect ratio versus thickness ratio for constant $A(t/c)^{1/3}$.

Figure 3.- Concluded.

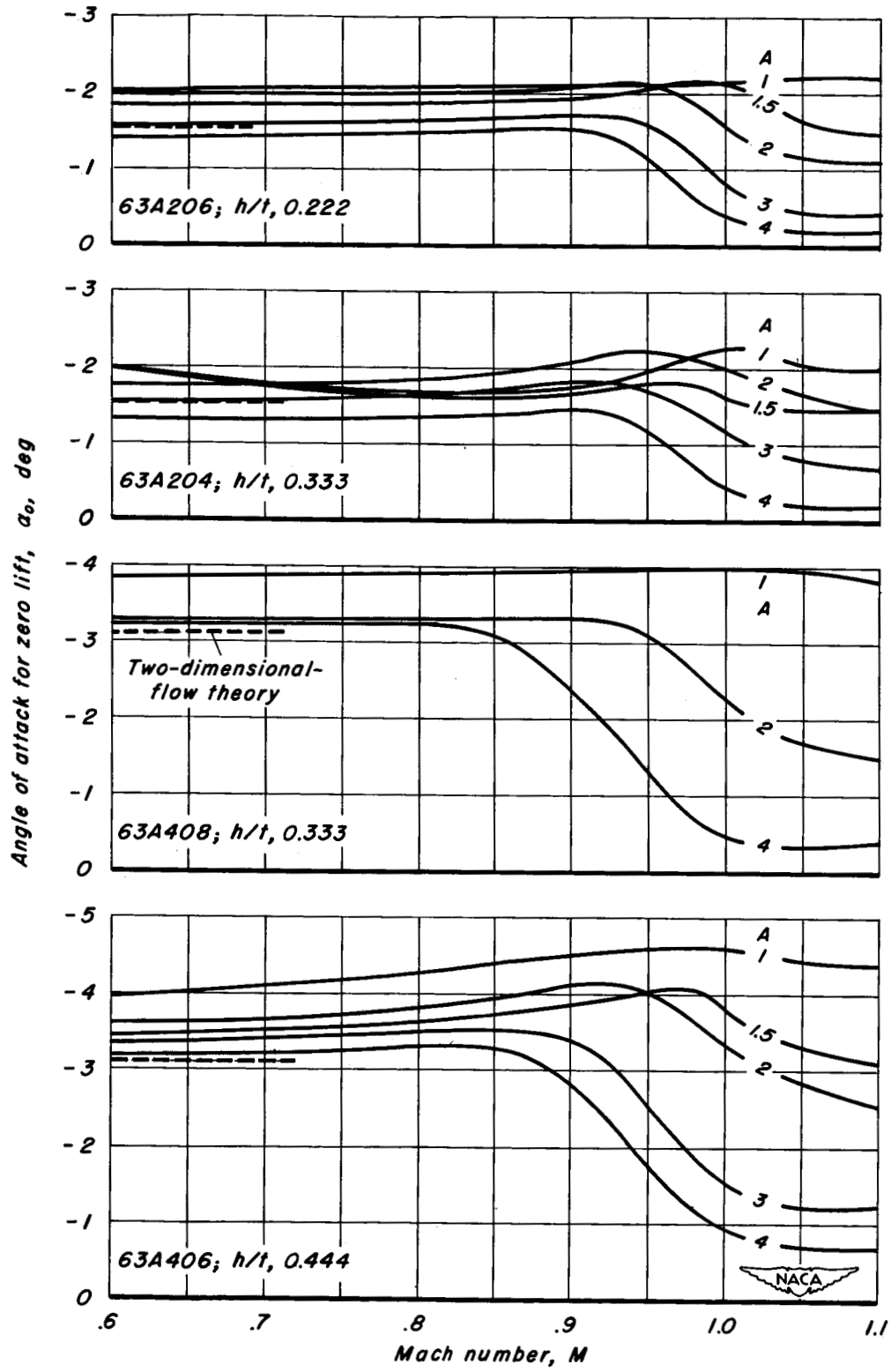

Figure 4.—The variation of the angle of attack for zero lift with Mach number.

[redacted]

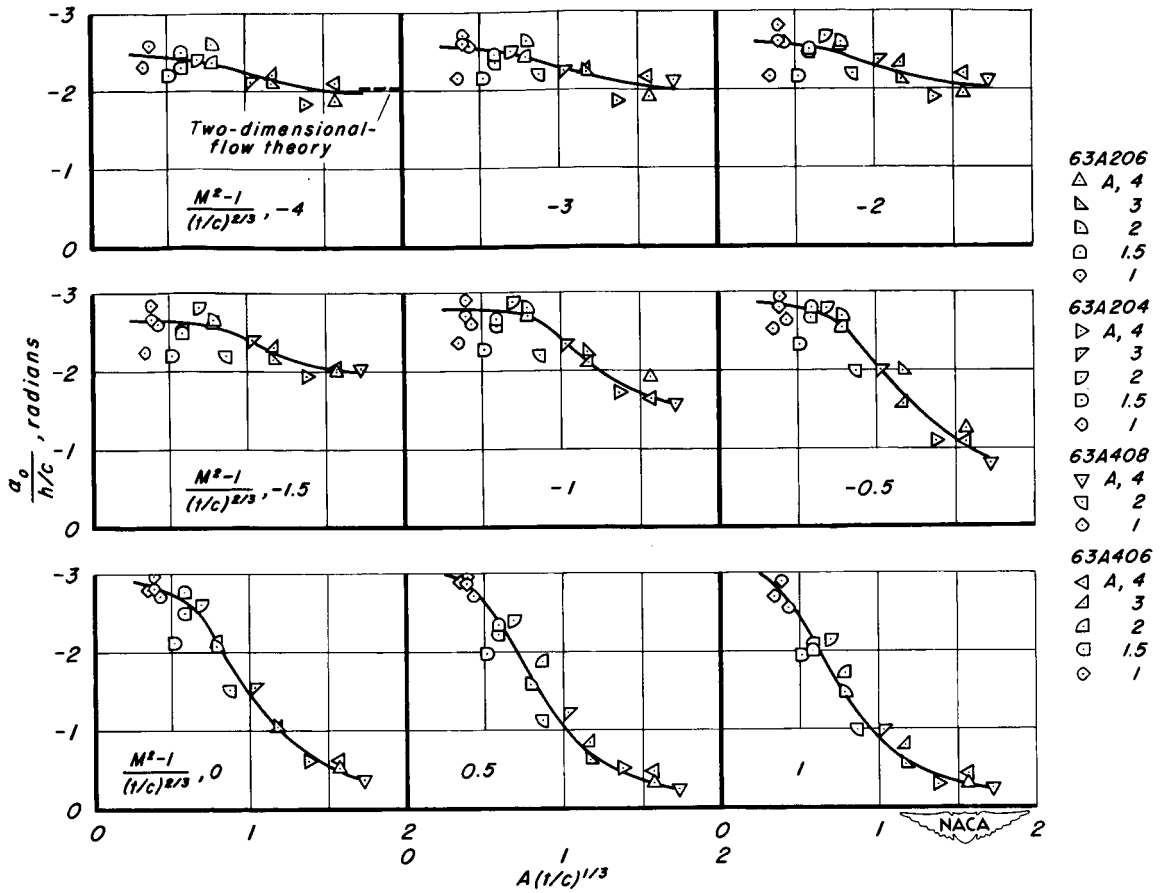

Figure 5.—Correlation of the generalized angle of attack for zero lift.

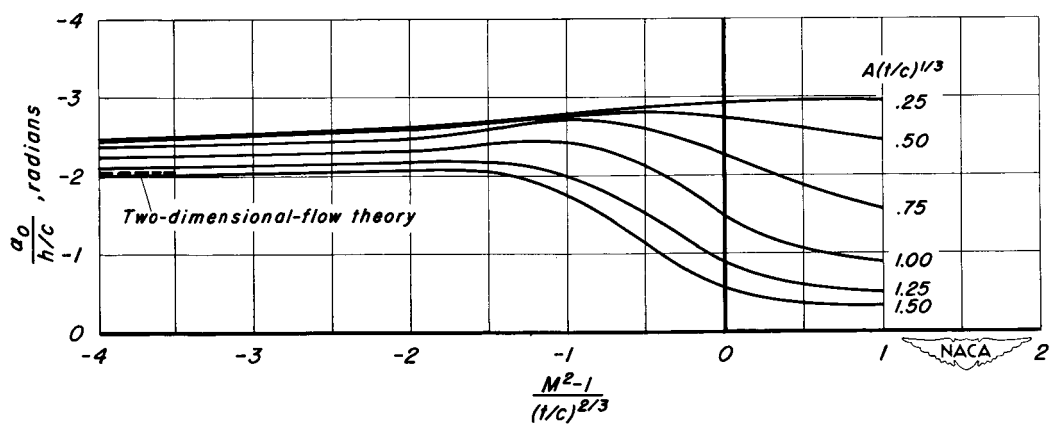

Figure 6.—Cross plot of the faired curves for the generalized angle of attack at zero lift for NACA 63AXXX airfoils with a=0.8 mean line.

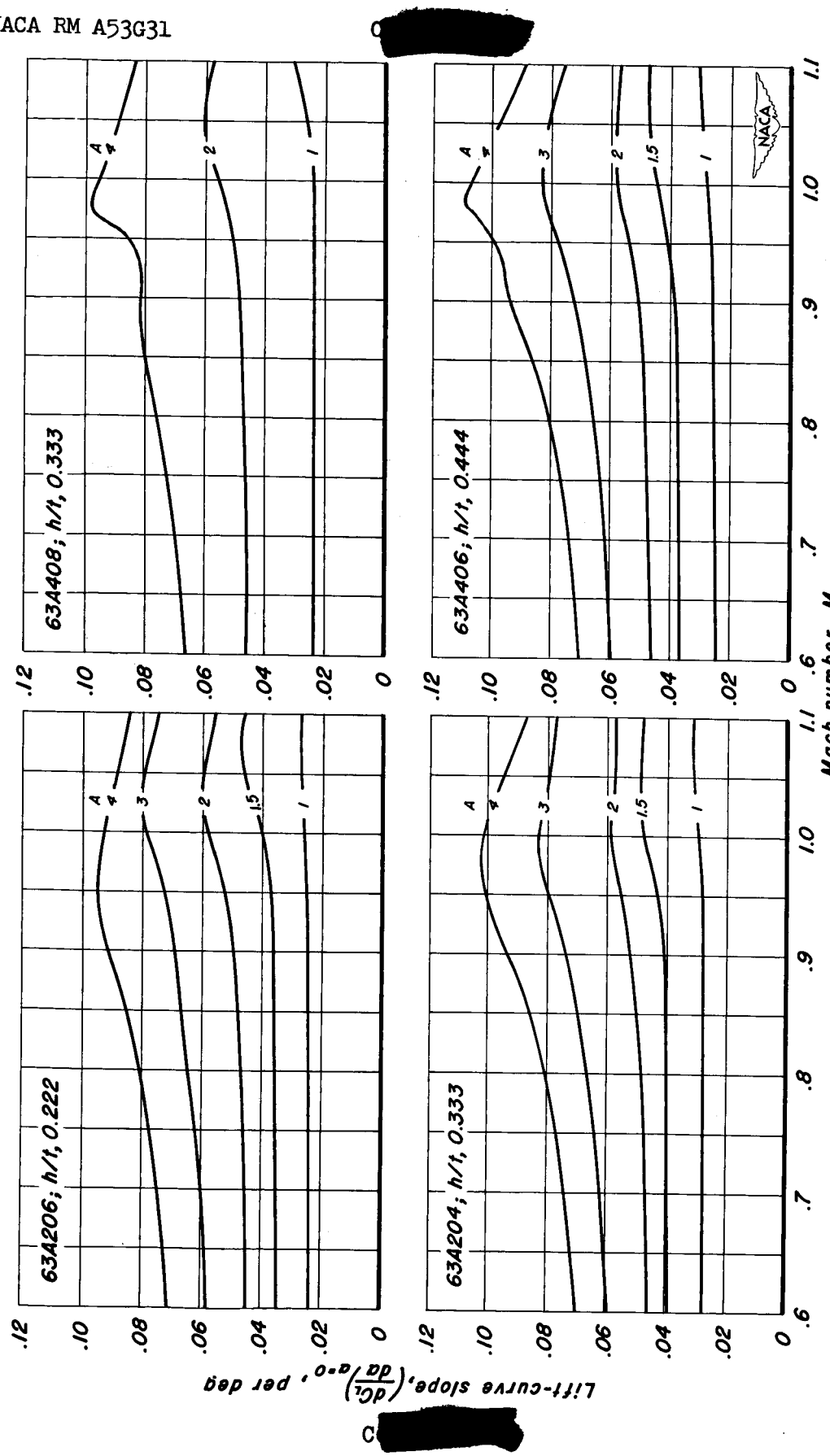

Figure 7.–The variation of lift-curve slope with Mach number.

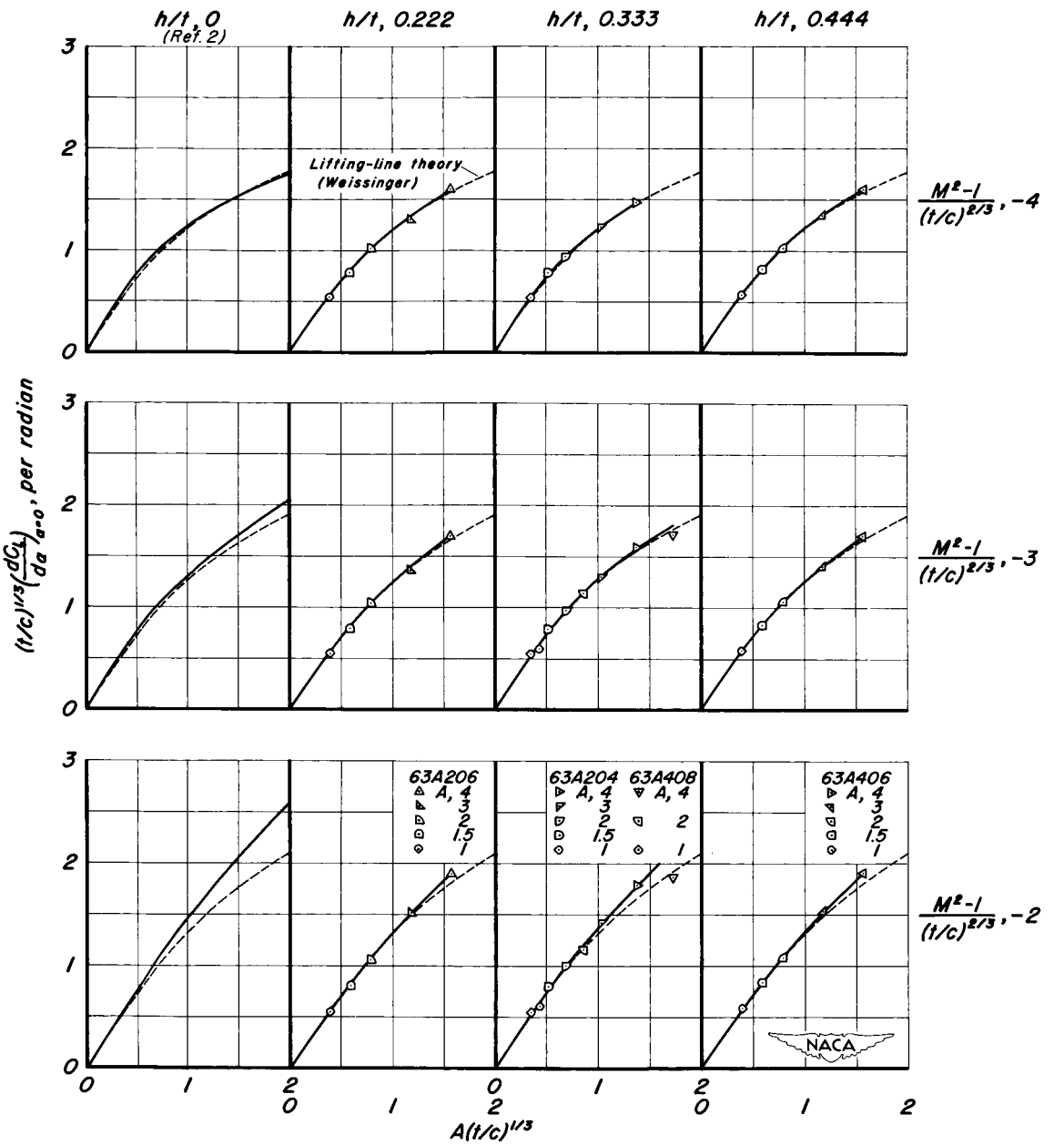

(a) $\frac{M^2-1}{(t/c)^{2/3}}$, -4, -3, and -2

Figure 8.- Correlation of the generalized lift-curve slope.

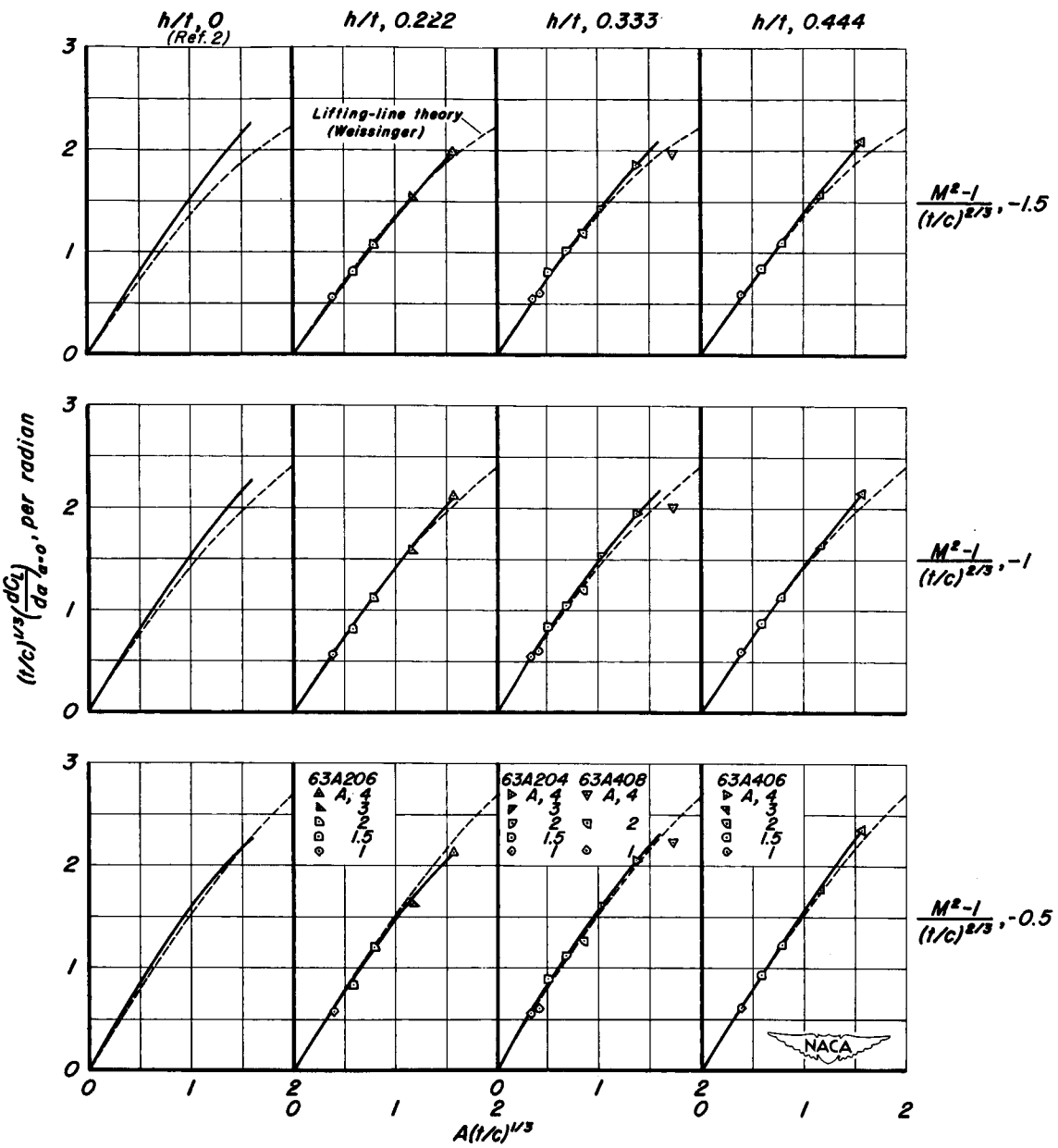

(b) $\frac{M^2-1}{(t/c)^{2/3}}$, -1.5, -1, and -0.5

Figure 8.- Continued.

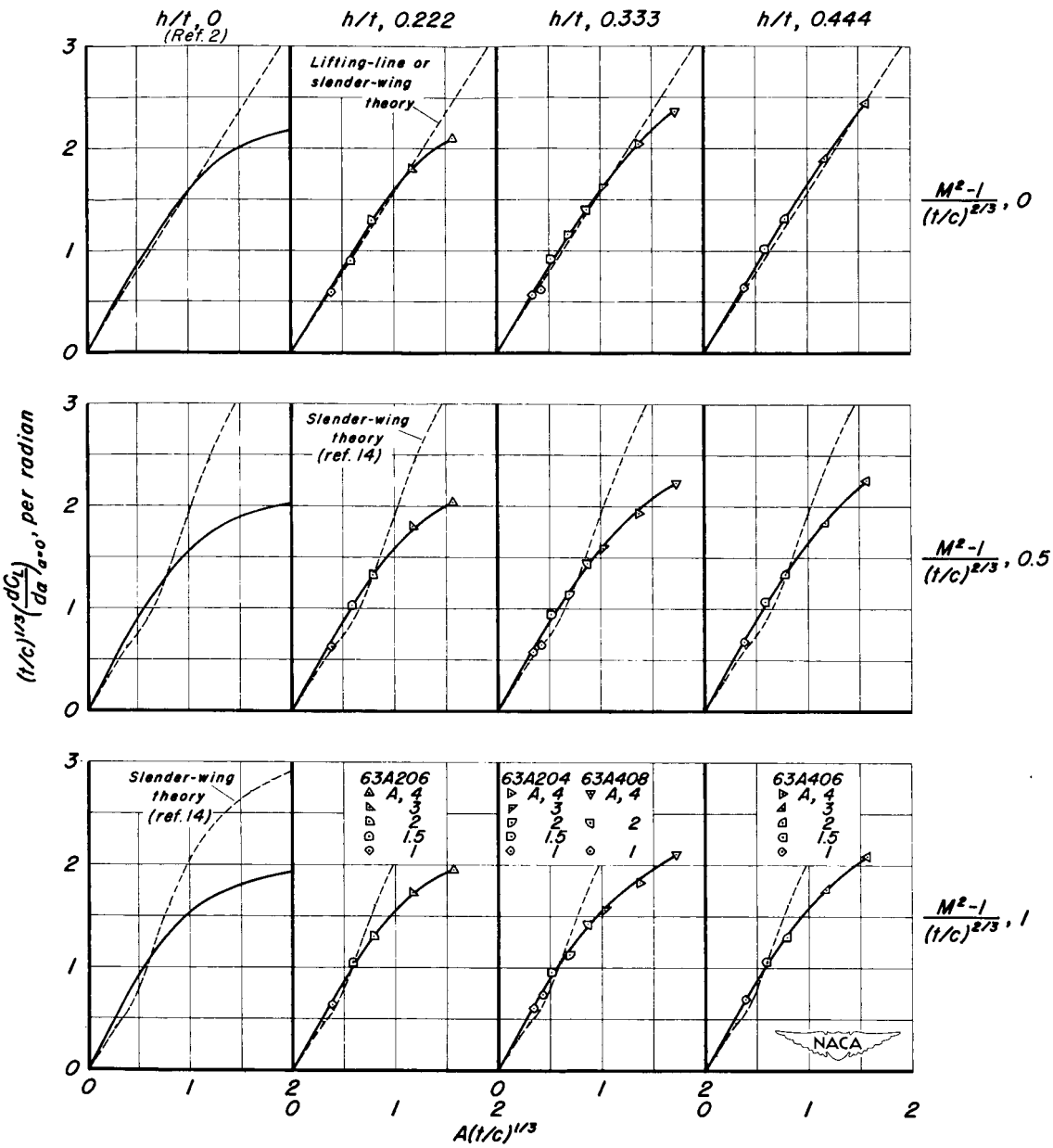

(c) $\frac{M^2-1}{(t/c)^{2/3}}$, 0, 0.5, and 1

Figure 8.- Concluded.

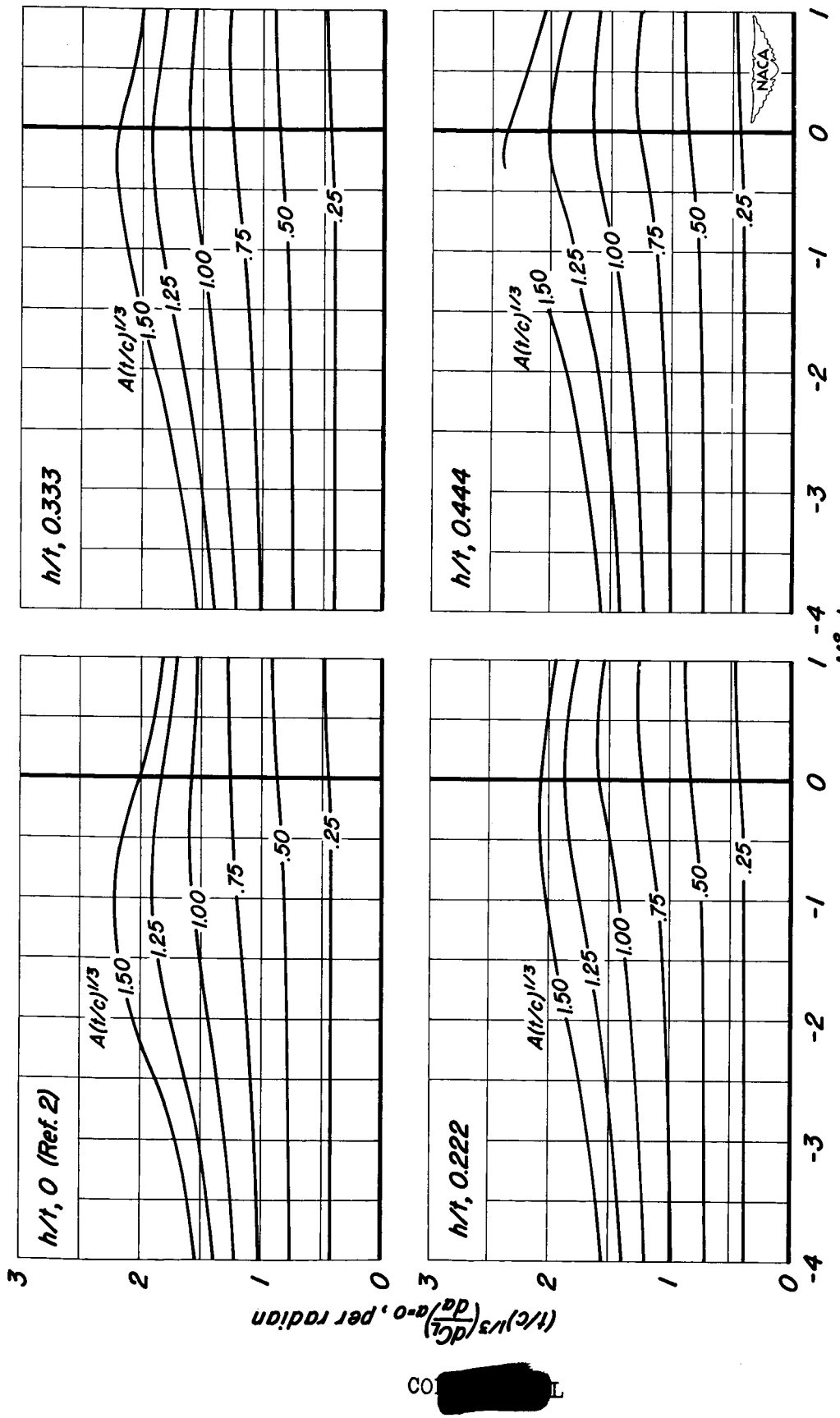

Figure 9.- Cross plot of the faired curves for the generalized lift-curve slope for NACA 63AXXX airfoils with a=0.8 mean line.

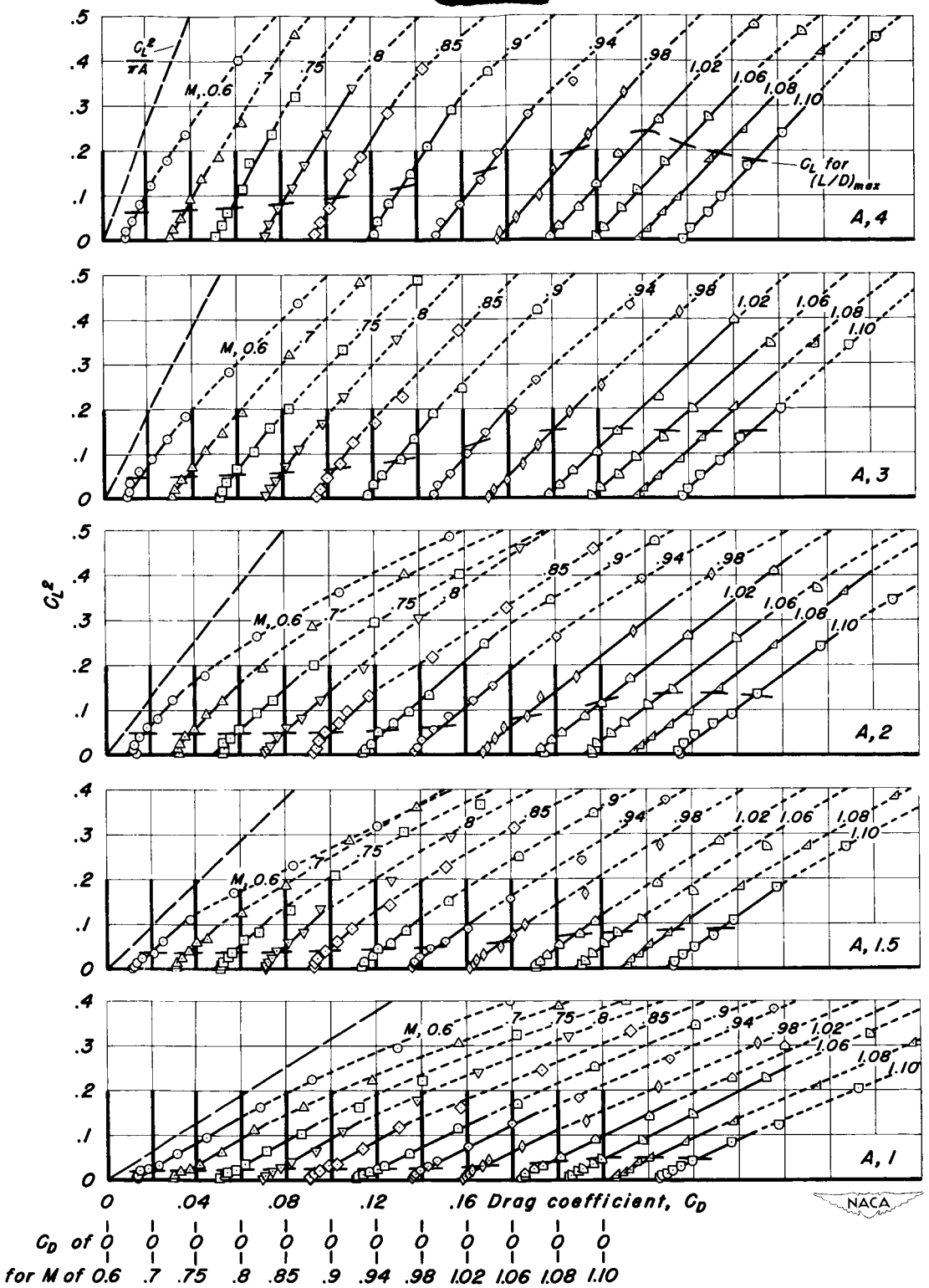

(a) NACA 63A206 section.

Figure 10.- The variation of drag coefficient with the square of the lift coefficient.

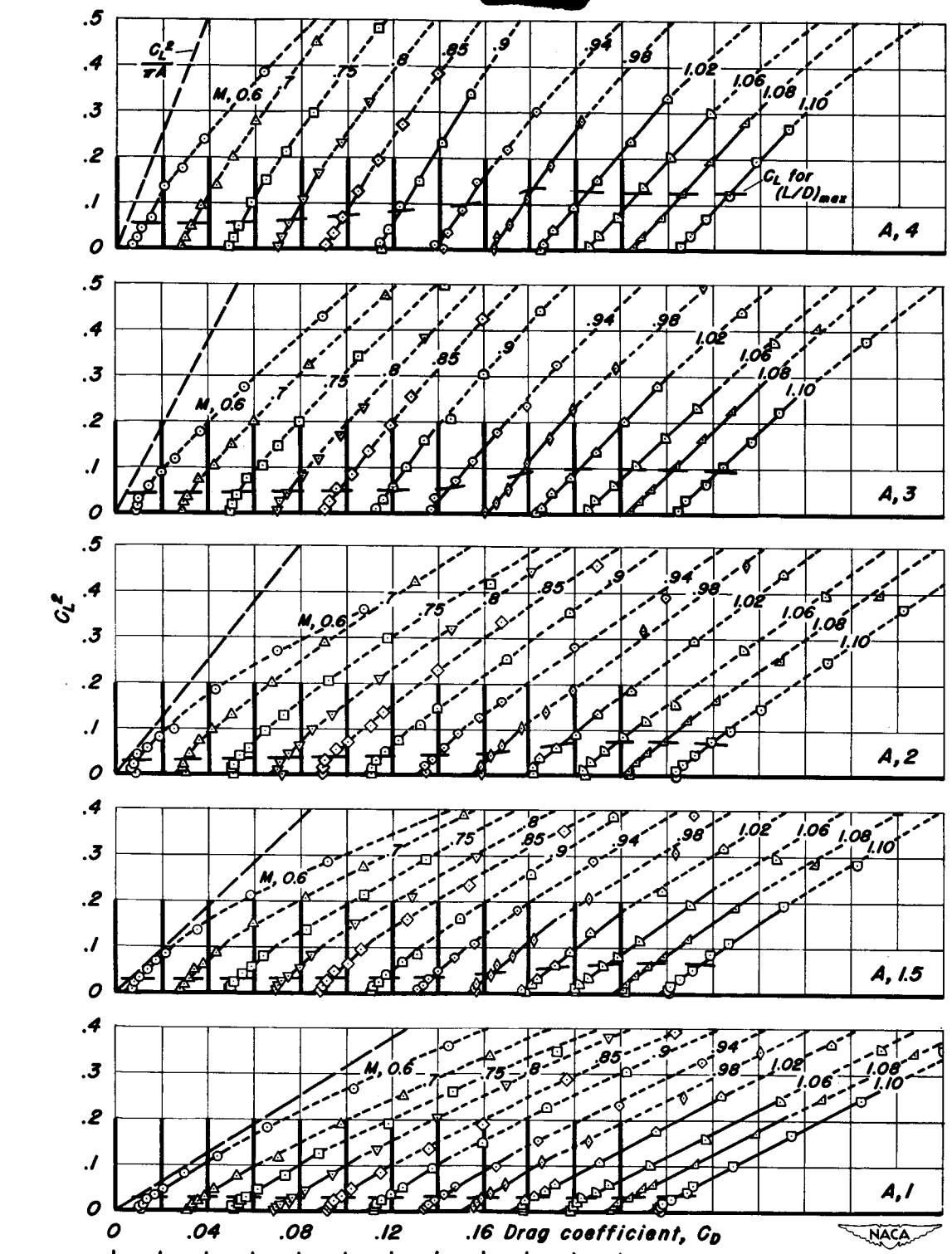

(b) NACA 63A204 section.

Figure 10.- Continued.

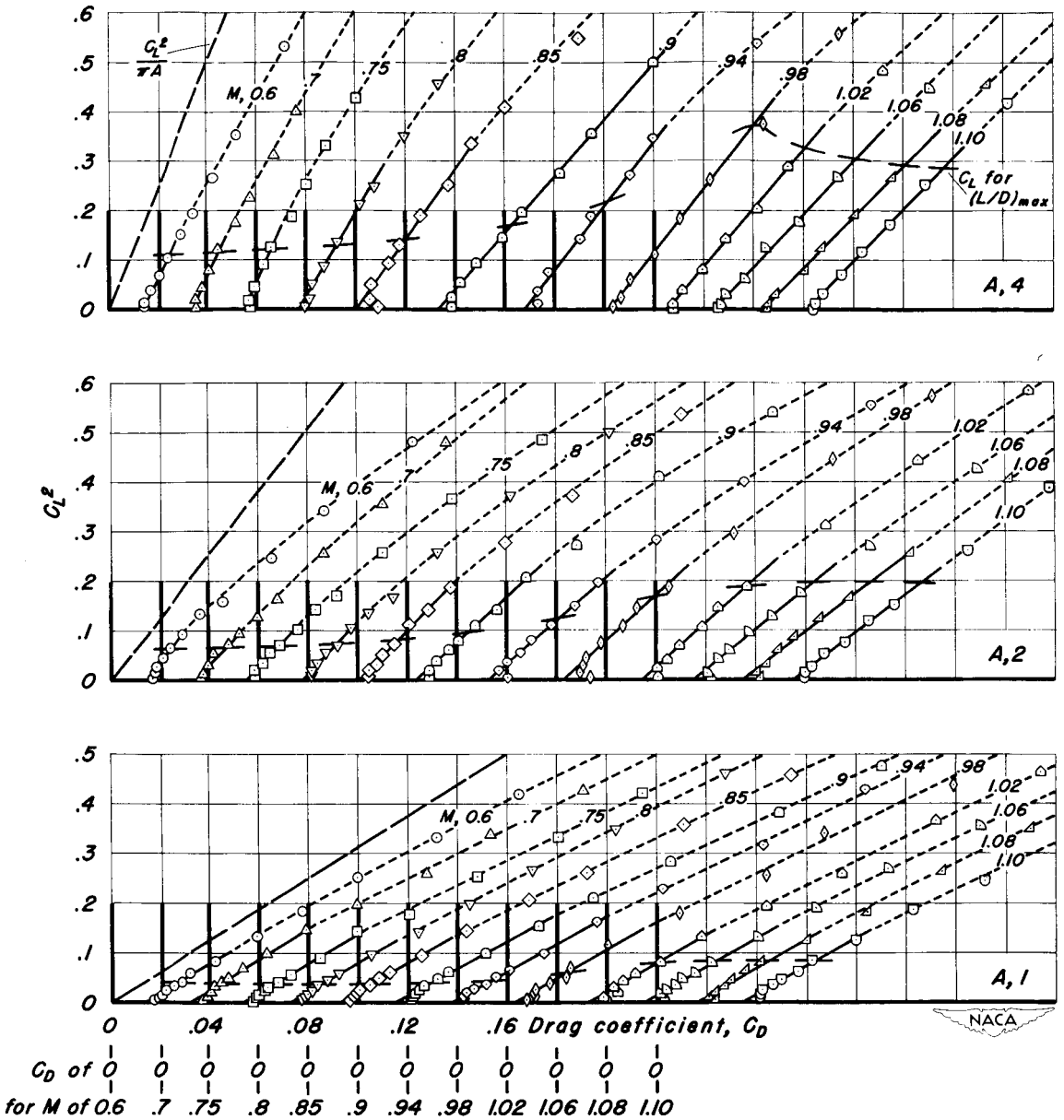

(c) NACA 63A408 section.

Figure 10.- Continued.

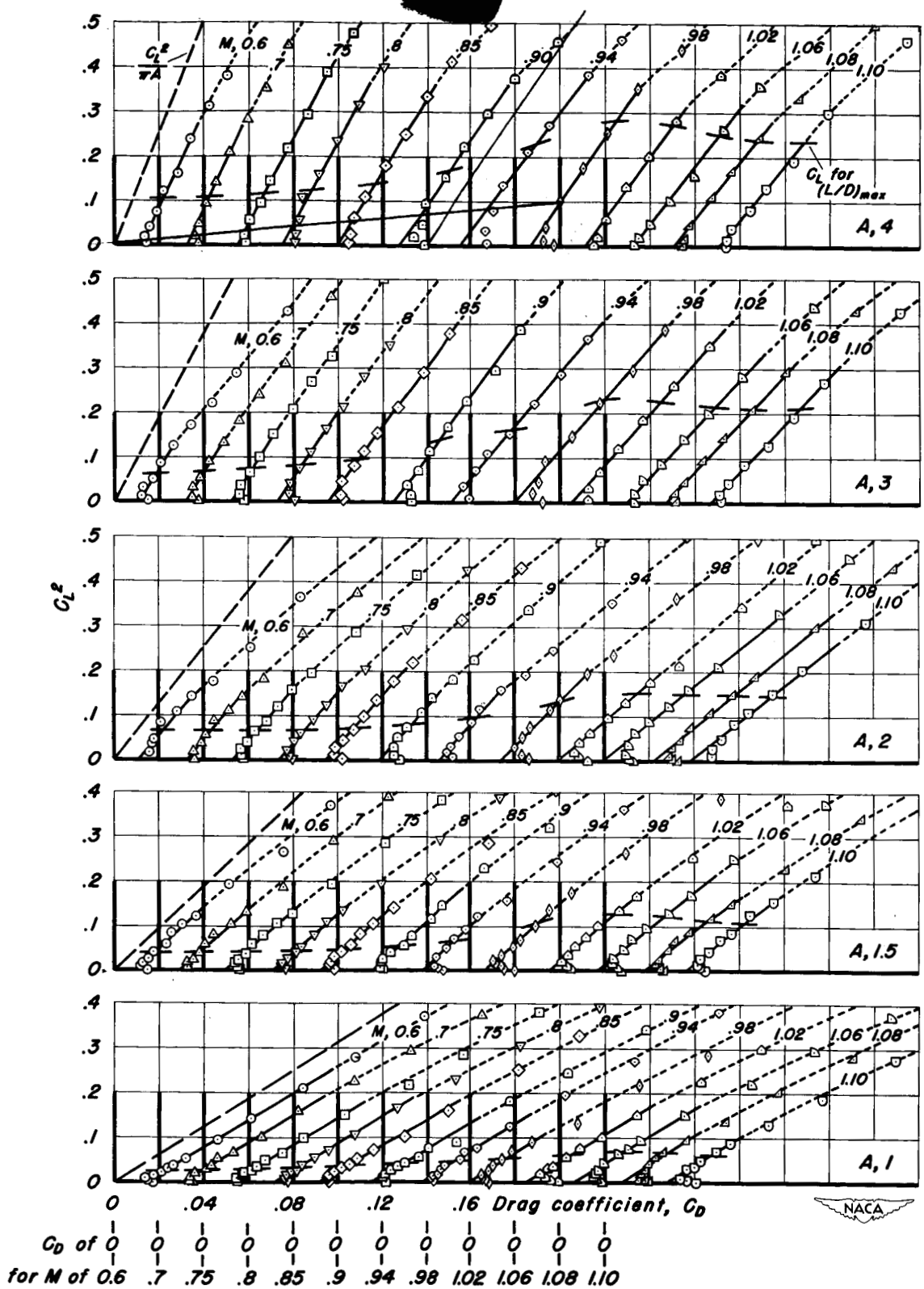

(d) NACA 63A406 section.

Figure 10.- Concluded.

[redacted]

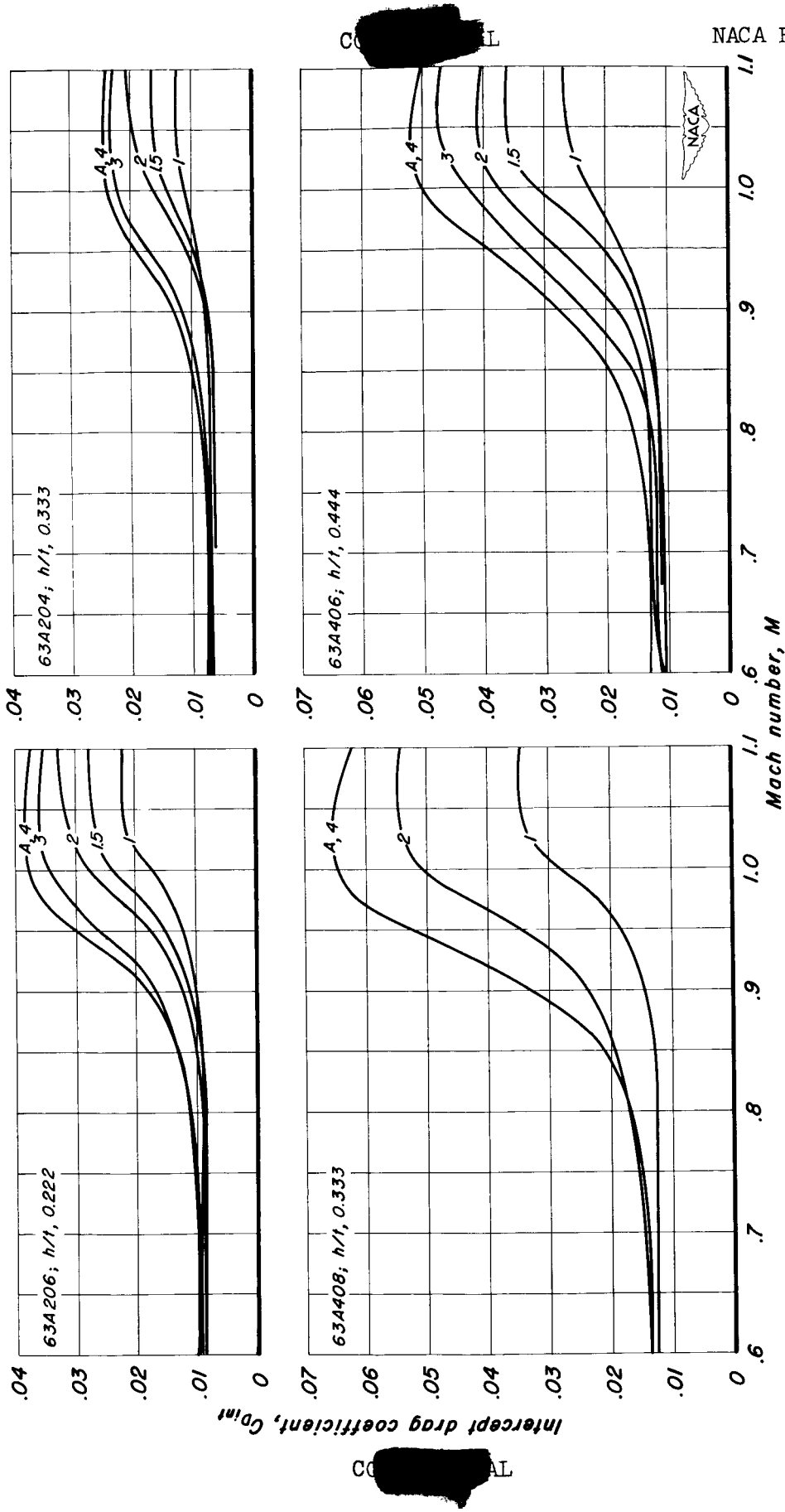

Figure 11.- The variation of intercept drag coefficient with Mach number.

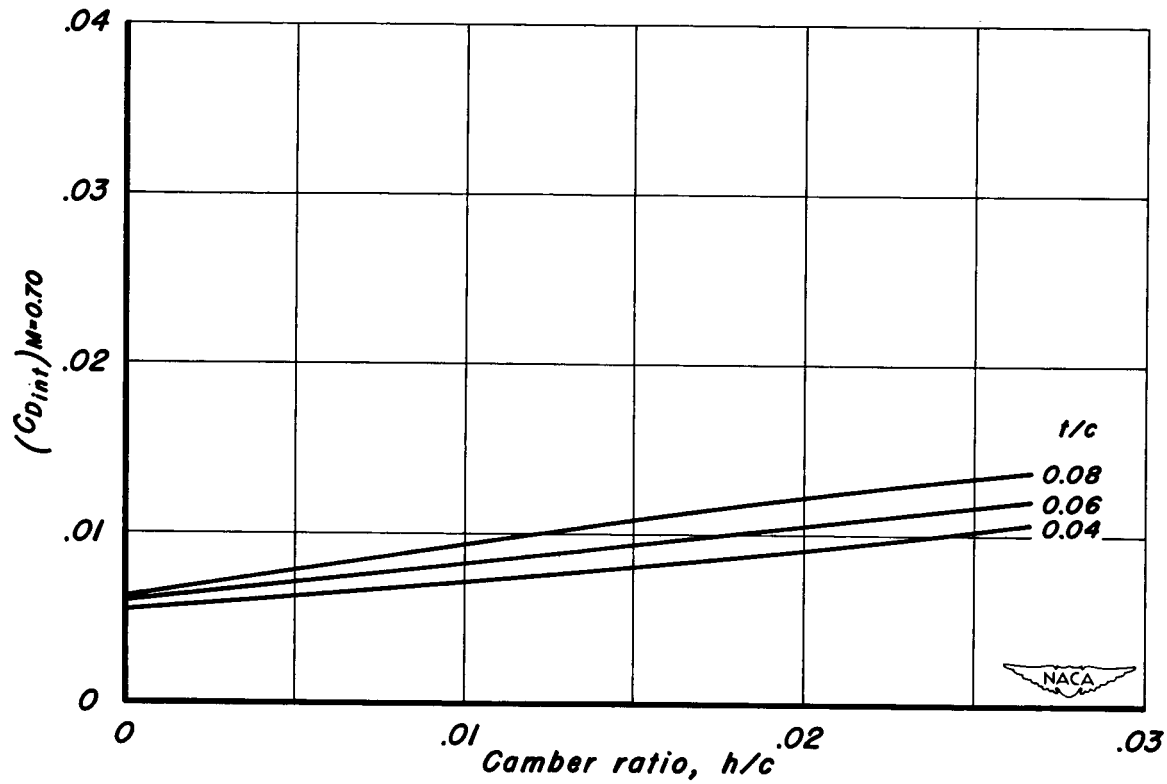

Figure 12.- The variation of the subcritical-intercept-drag coefficient, $C_{D_{int}}$ at 0.70 Mach number, with camber-to-chord ratio.

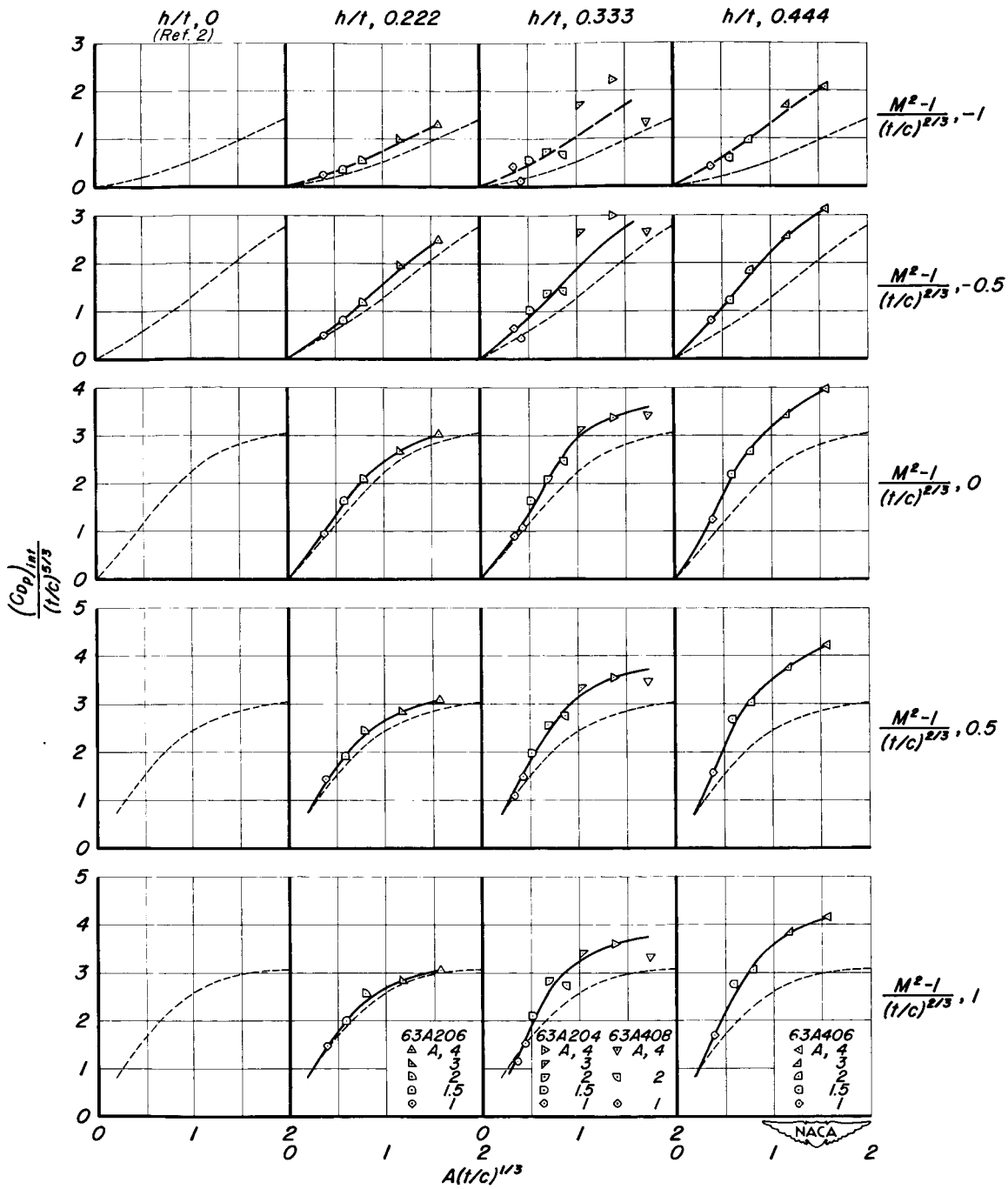

Figure 13.- Correlation of the generalized intercept pressure-drag coefficient.

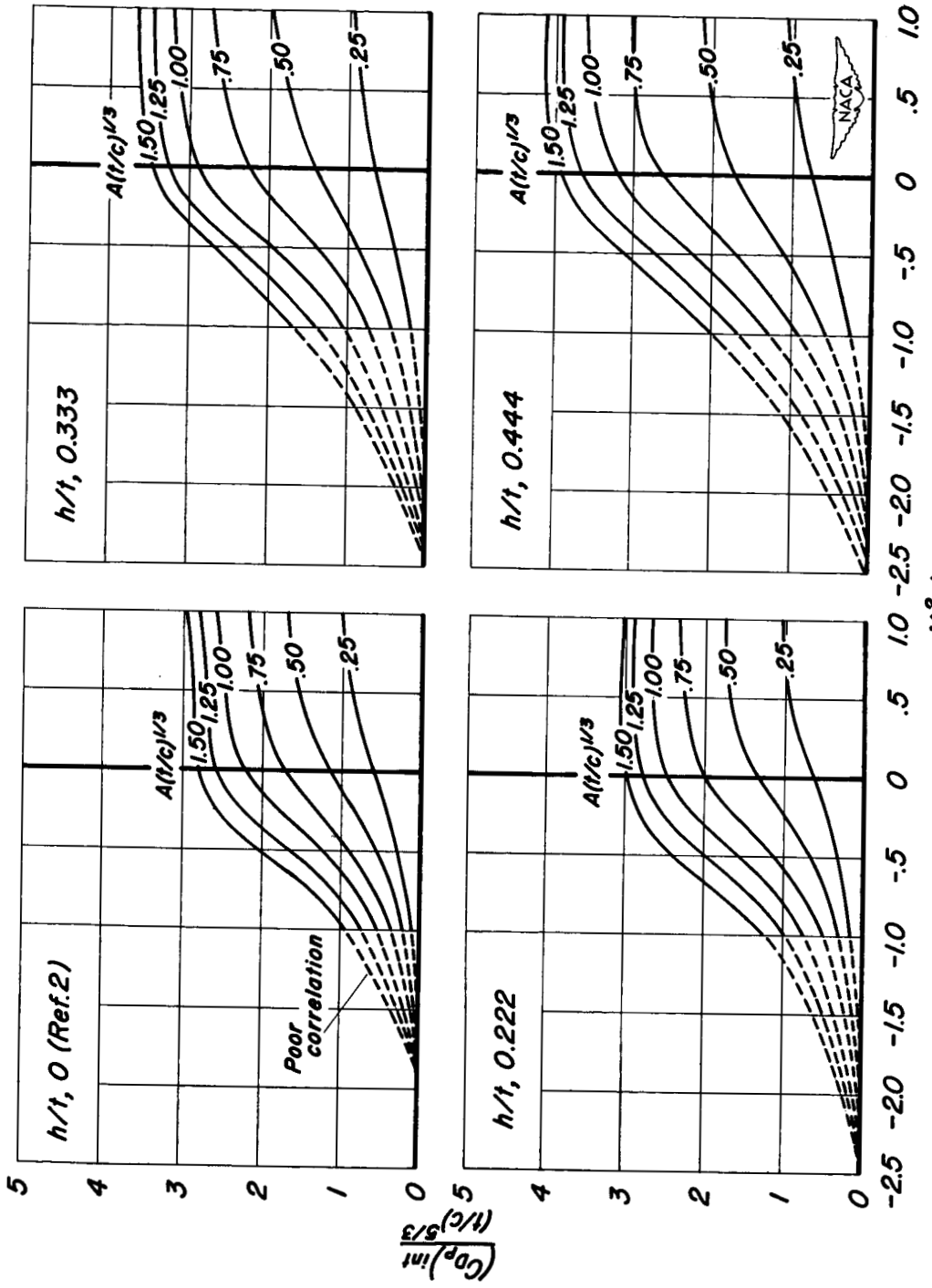

Figure 14.- Cross plot of the faired curves for the generalized intercept pressure-drag coefficient for NACA 63AXXX airfoils with a=0.8 mean line.

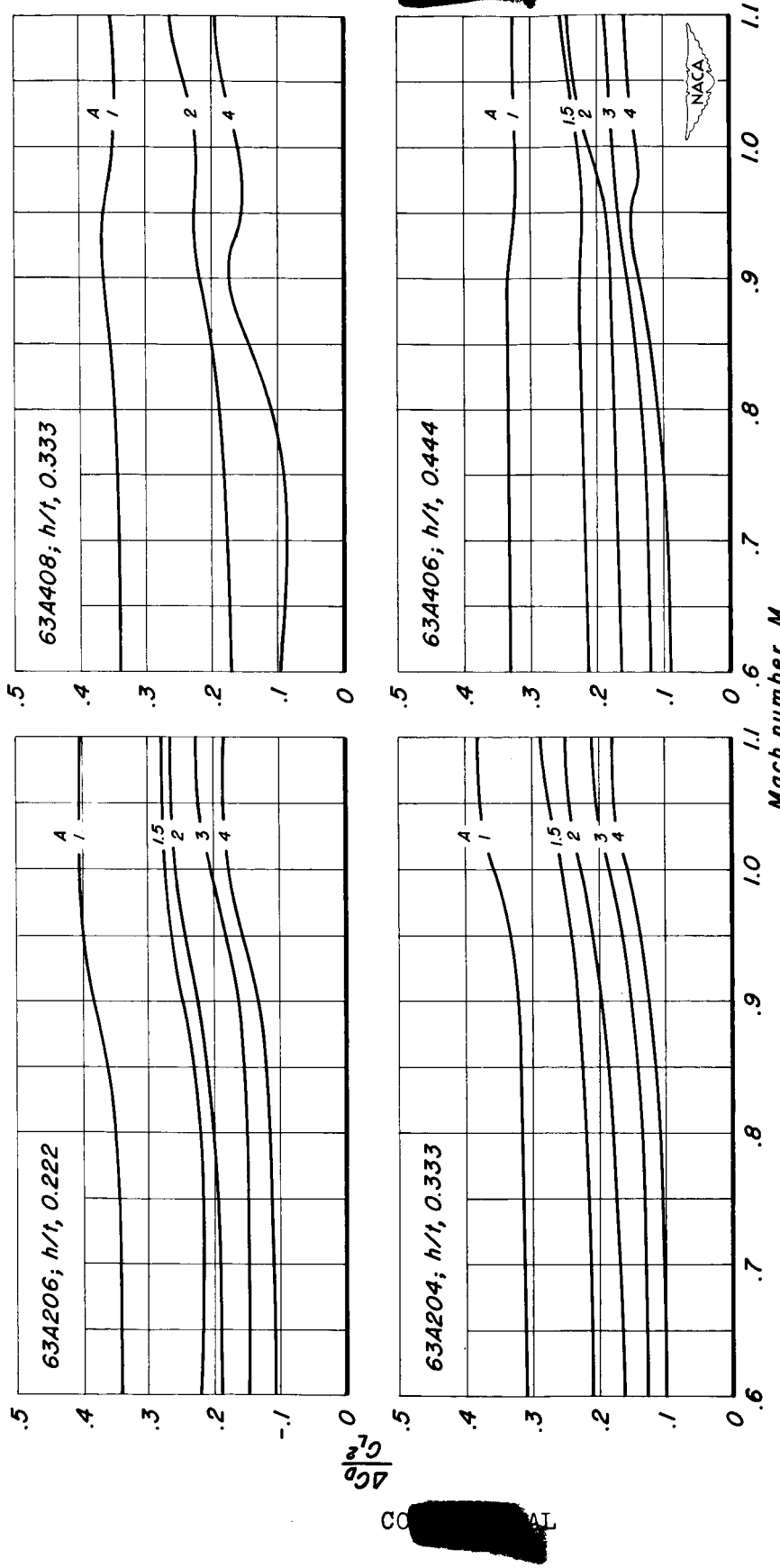

Figure 15.- The variation of the drag-due-to-lift parameter with Mach number.

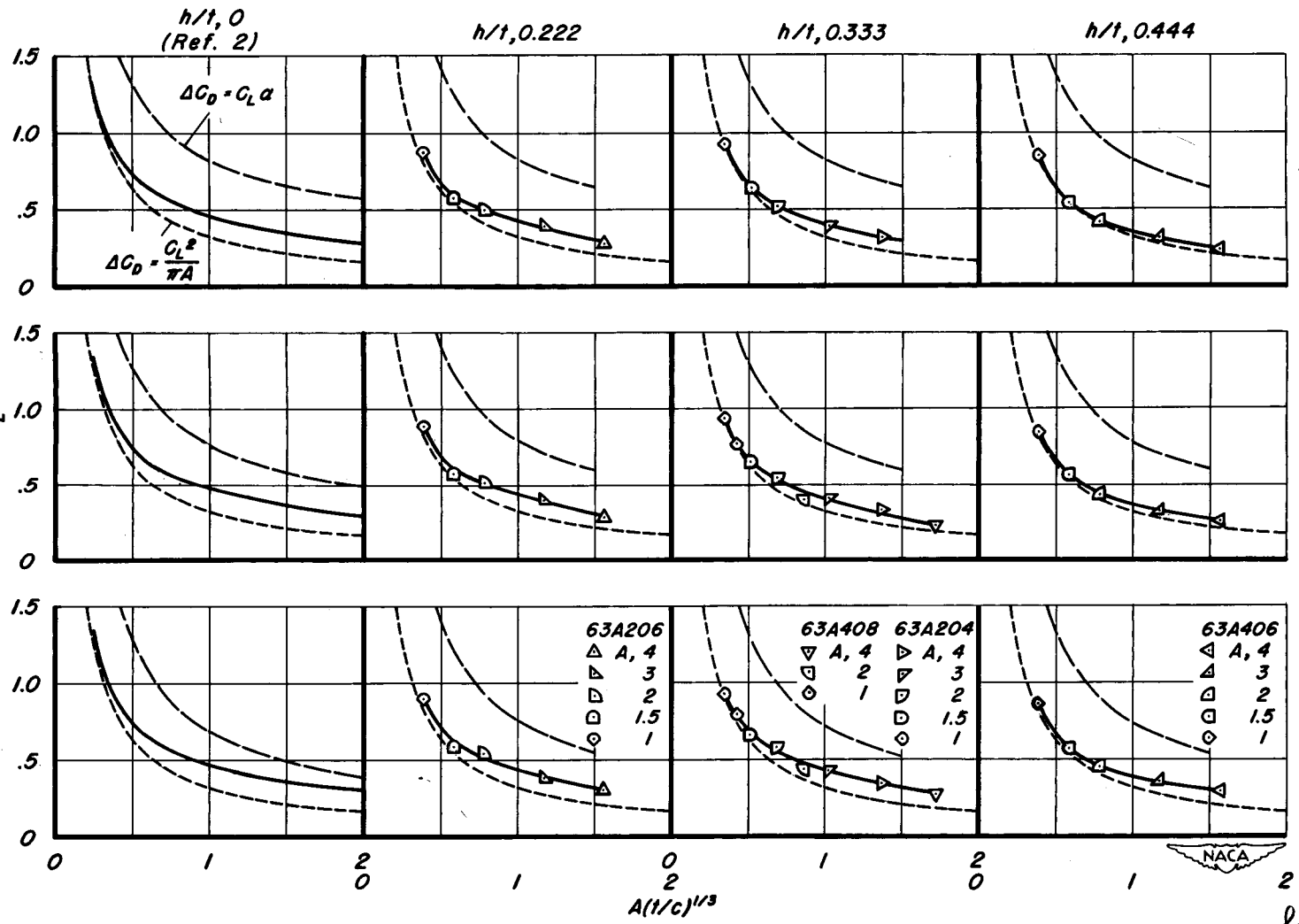

(a) $\frac{M^2-1}{(t/c)^{2/3}}$, -4, -3, and -2

Figure 16.-Correlation of the generalized drag-due-to-lift coefficient.

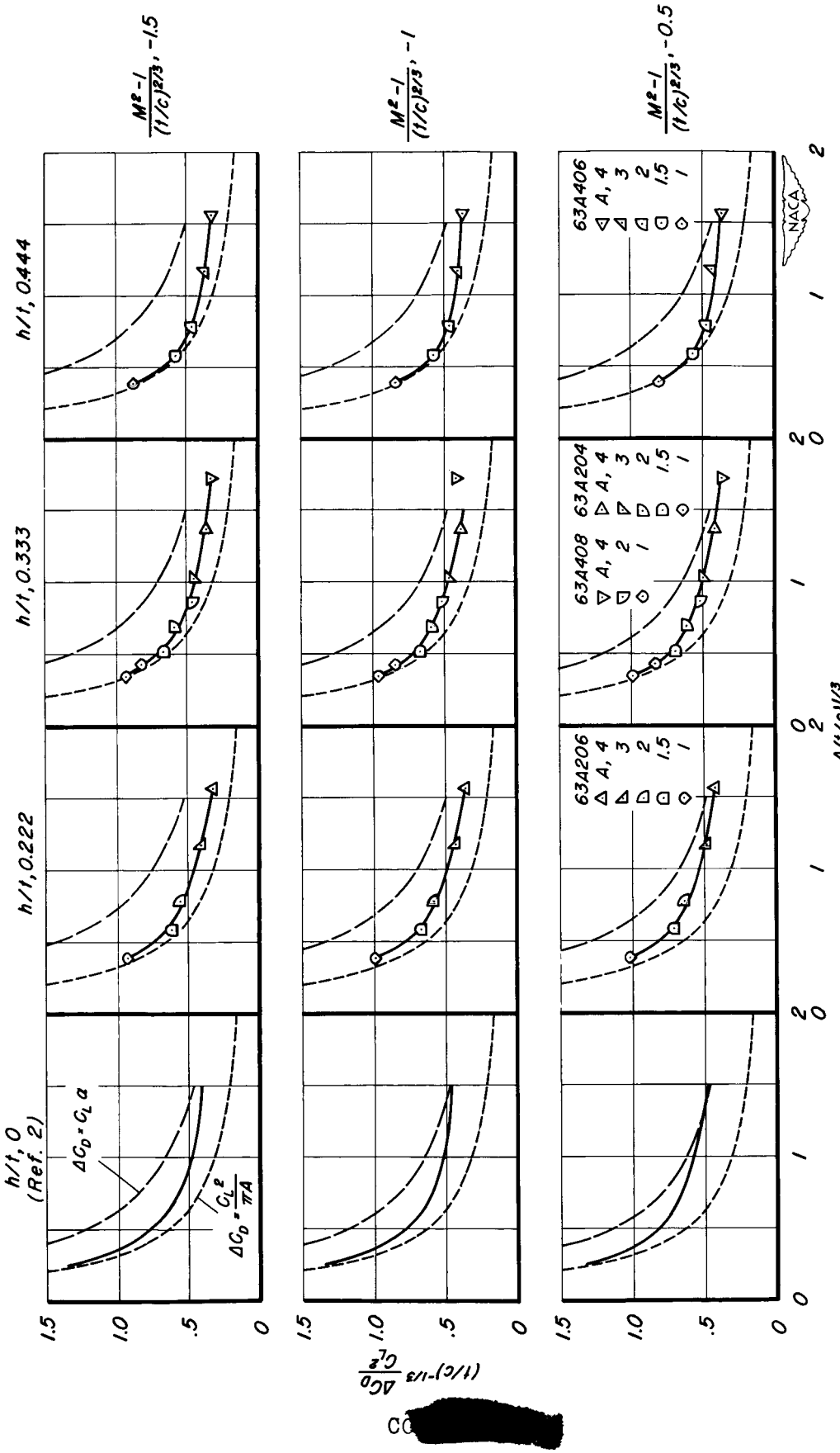

(b) $\frac{M^2-1}{(t/c)^{2/3}}$, -1.5, -1, and, -0.5

Figure 16.-Continued.

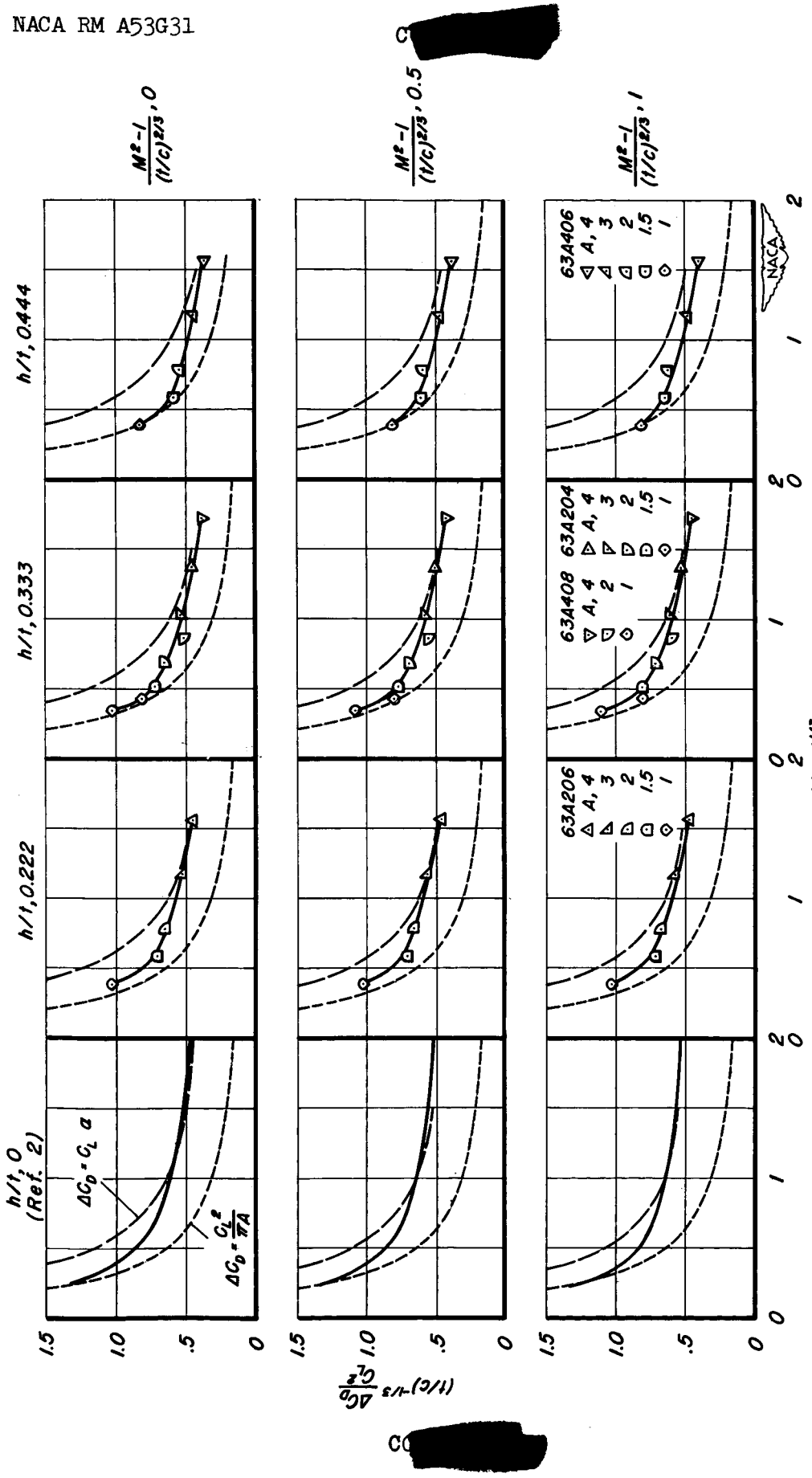

(c) $\frac{M^2-1}{(t/c)^{2/3}}$, 0, 0.5, and 1

Figure 16.- Concluded.

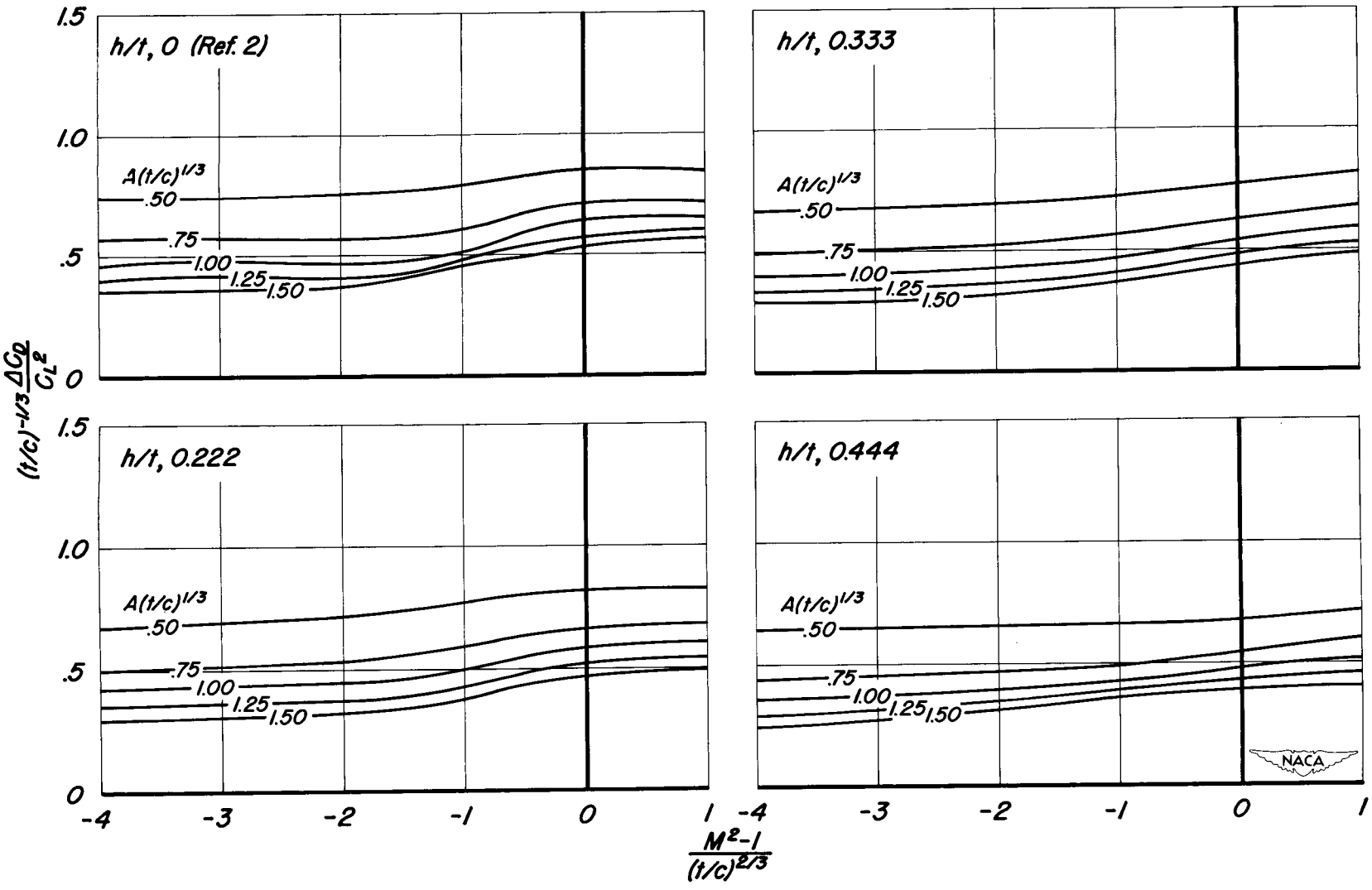

Figure 17.- Cross plot of the faired curves for the generalized drag-due-to-lift coefficient for NACA 63AXXX airfoils with a=0.8 mean line.

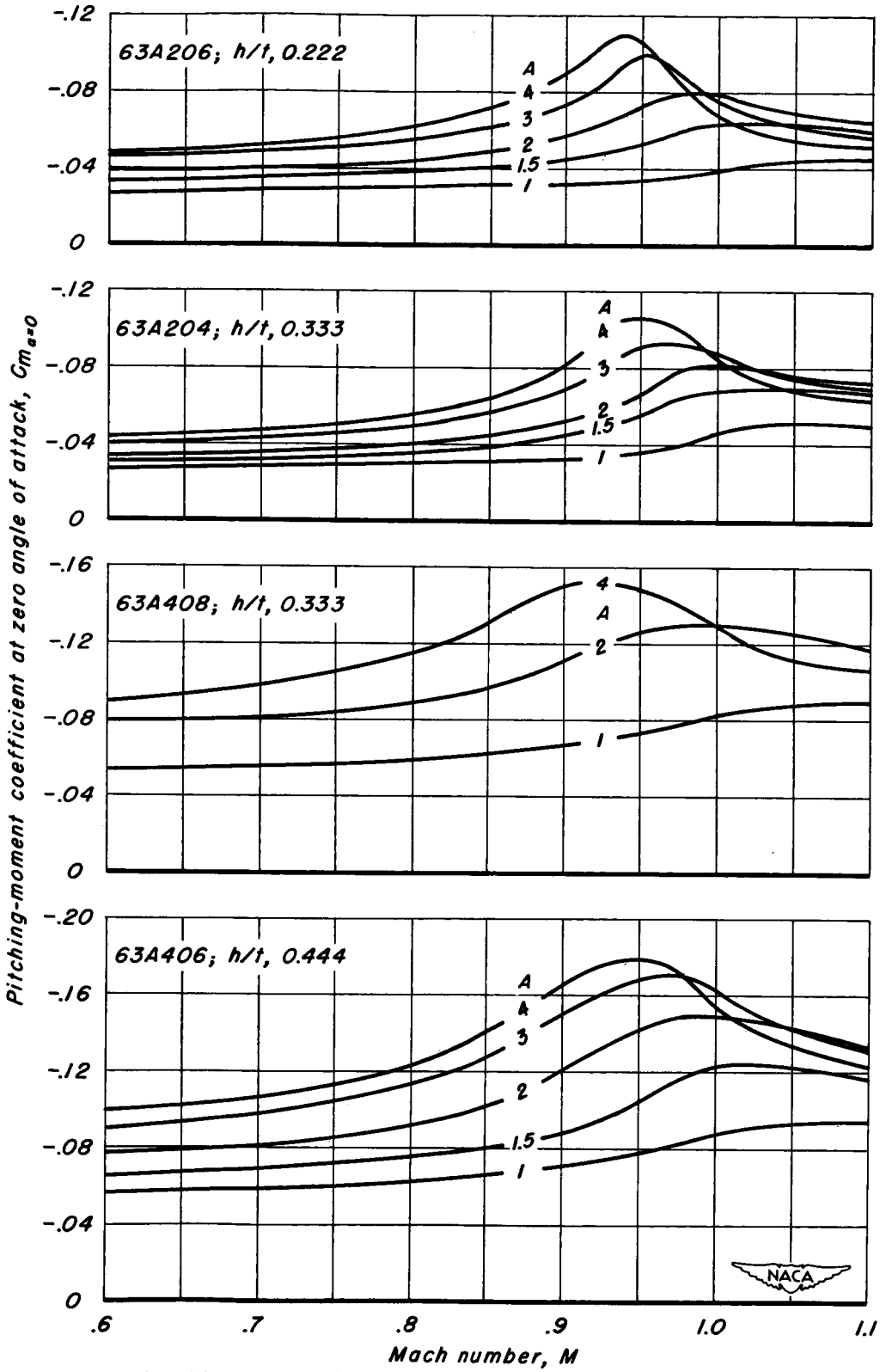

Figure 18.—The variation of pitching-moment coefficient for zero lift with Mach number.

C[redacted]

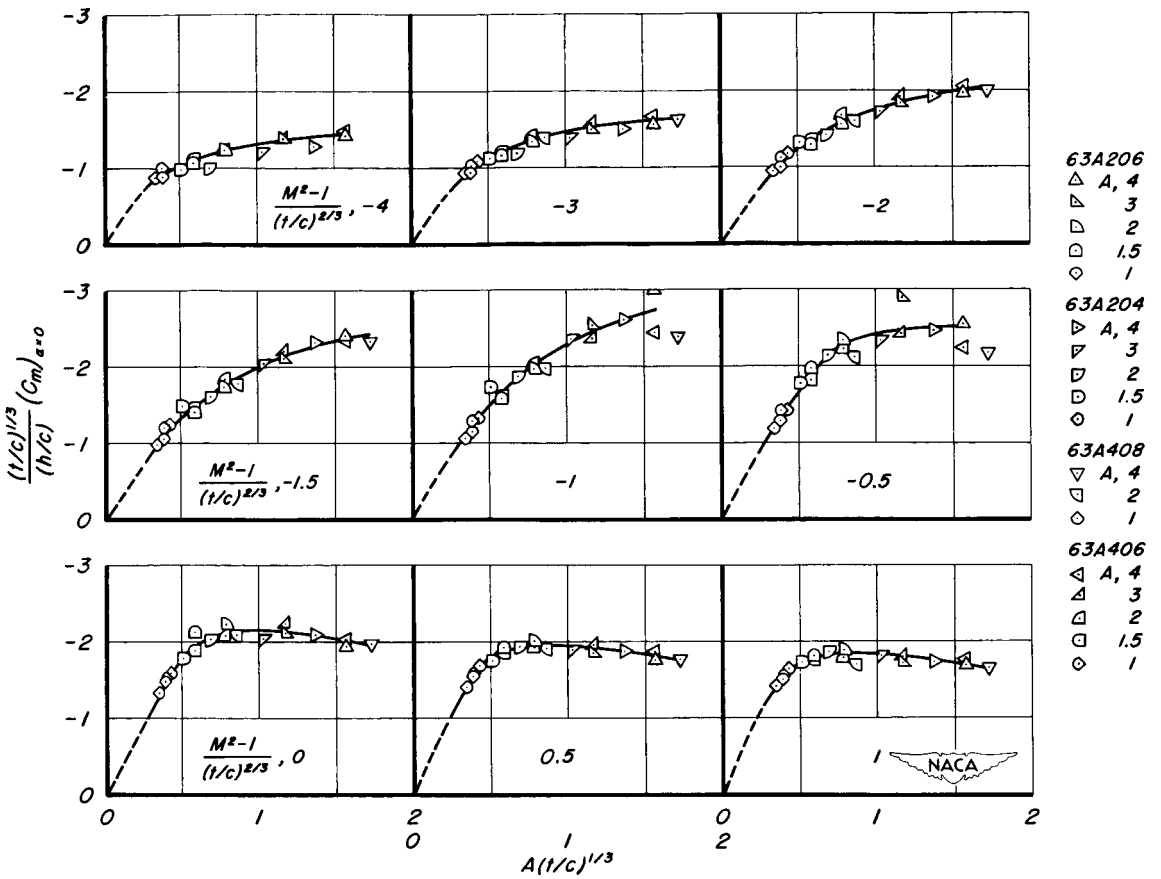

Figure 19.- Correlation of the generalized pitching-moment coefficient for zero angle of attack.

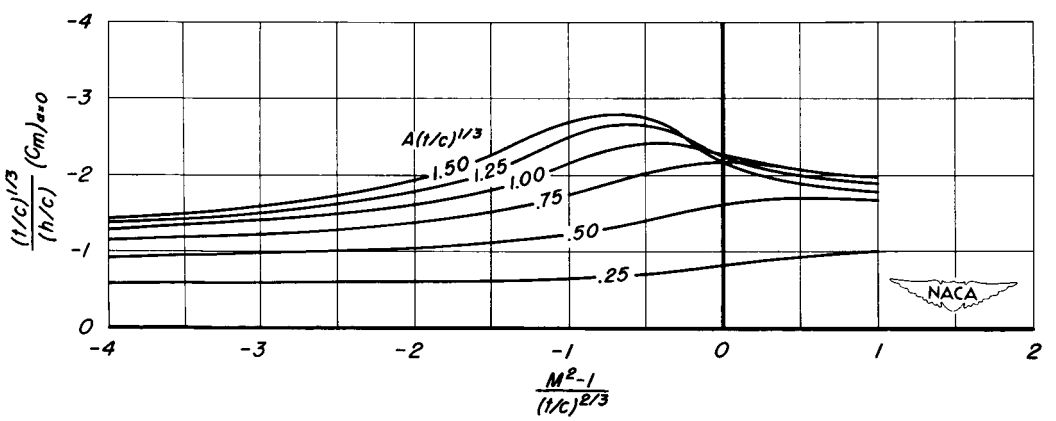

Figure 20.-Cross plot of the faired curves for the generalized pitching-moment coefficient at zero angle of attack for NACA 63AXXX airfoils with a=0.8 mean line.

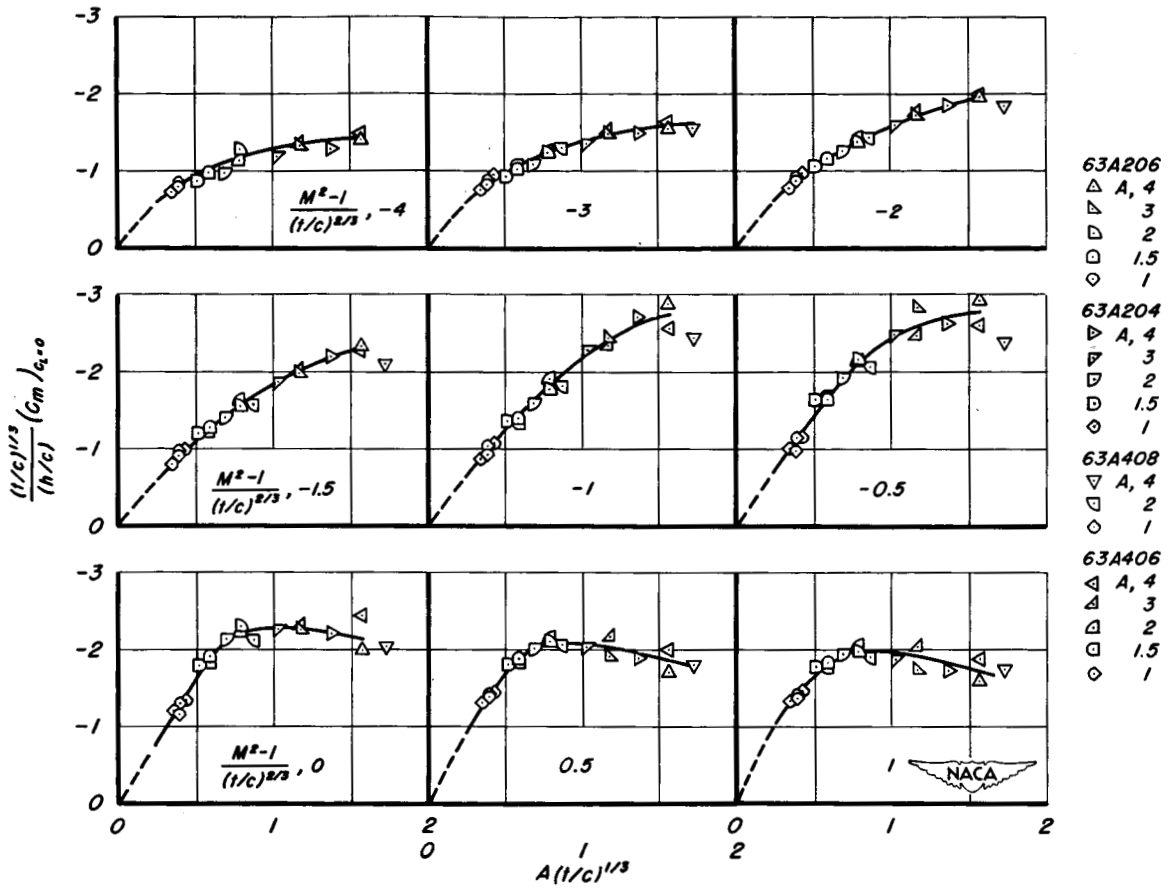

Figure 21.- Correlation of the generalized pitching-moment coefficient for zero lift.

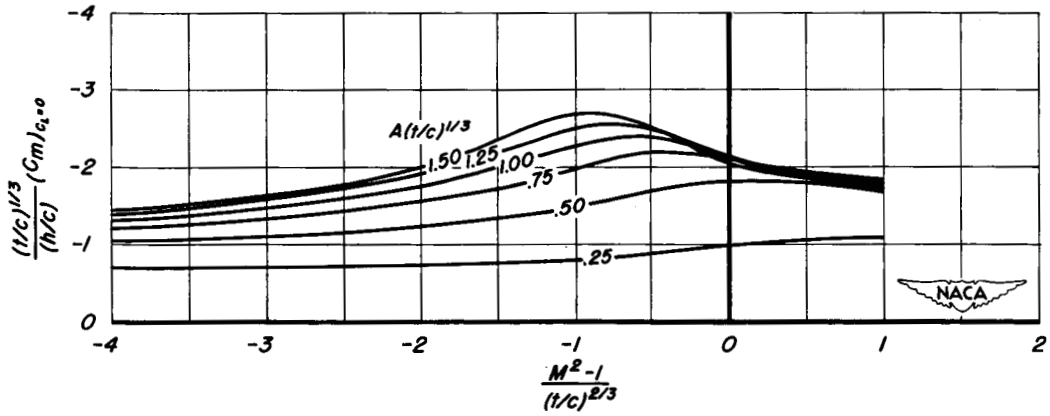

Figure 22.-Cross plot of the faired curves for the generalized pitching-moment coefficient at zero lift for NACA 63AXXX airfoils with a = 0.8 mean line.

[redacted]

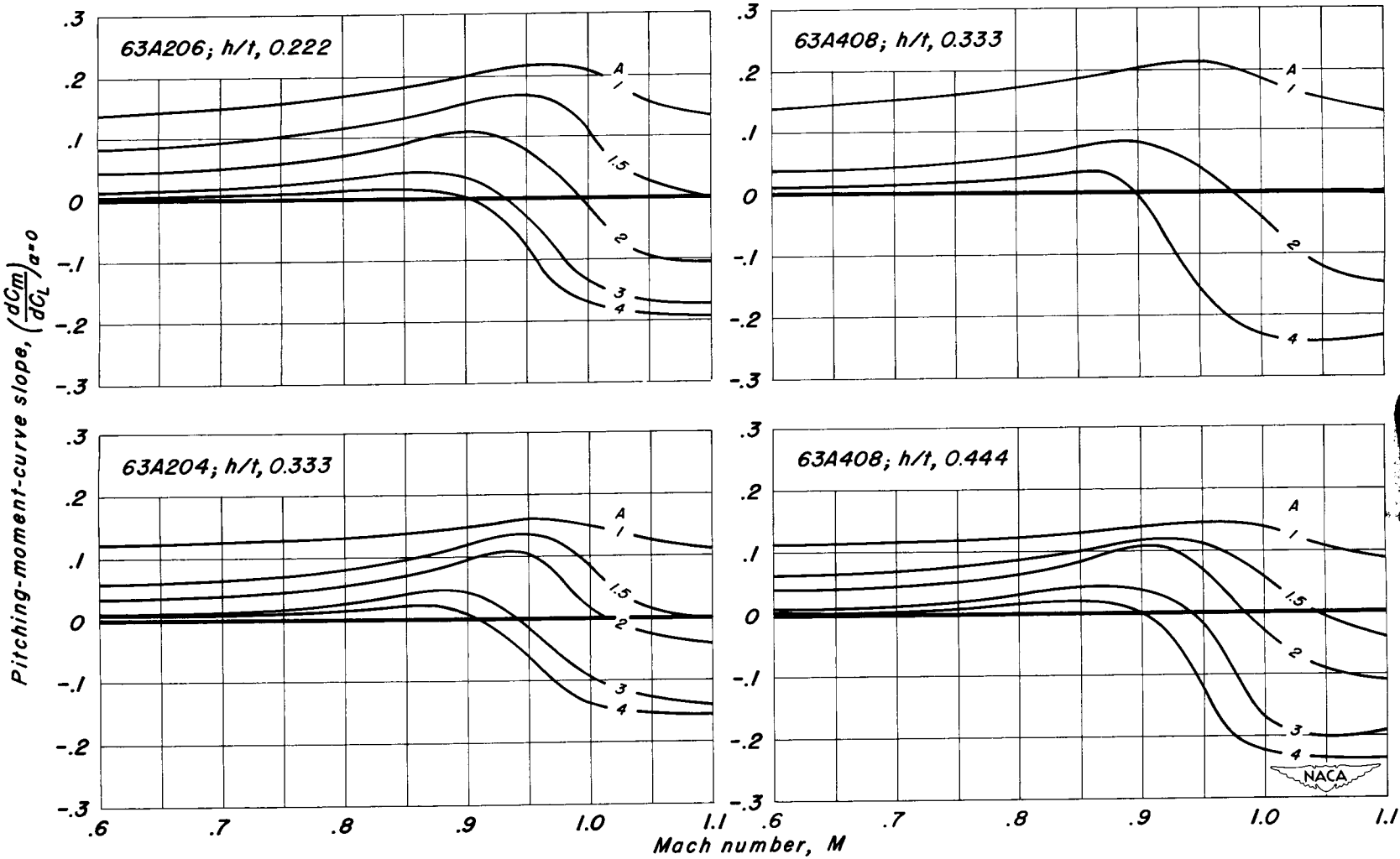

Figure 23.–The variation of pitching-moment-curve slope with Mach number. $\alpha=0$.

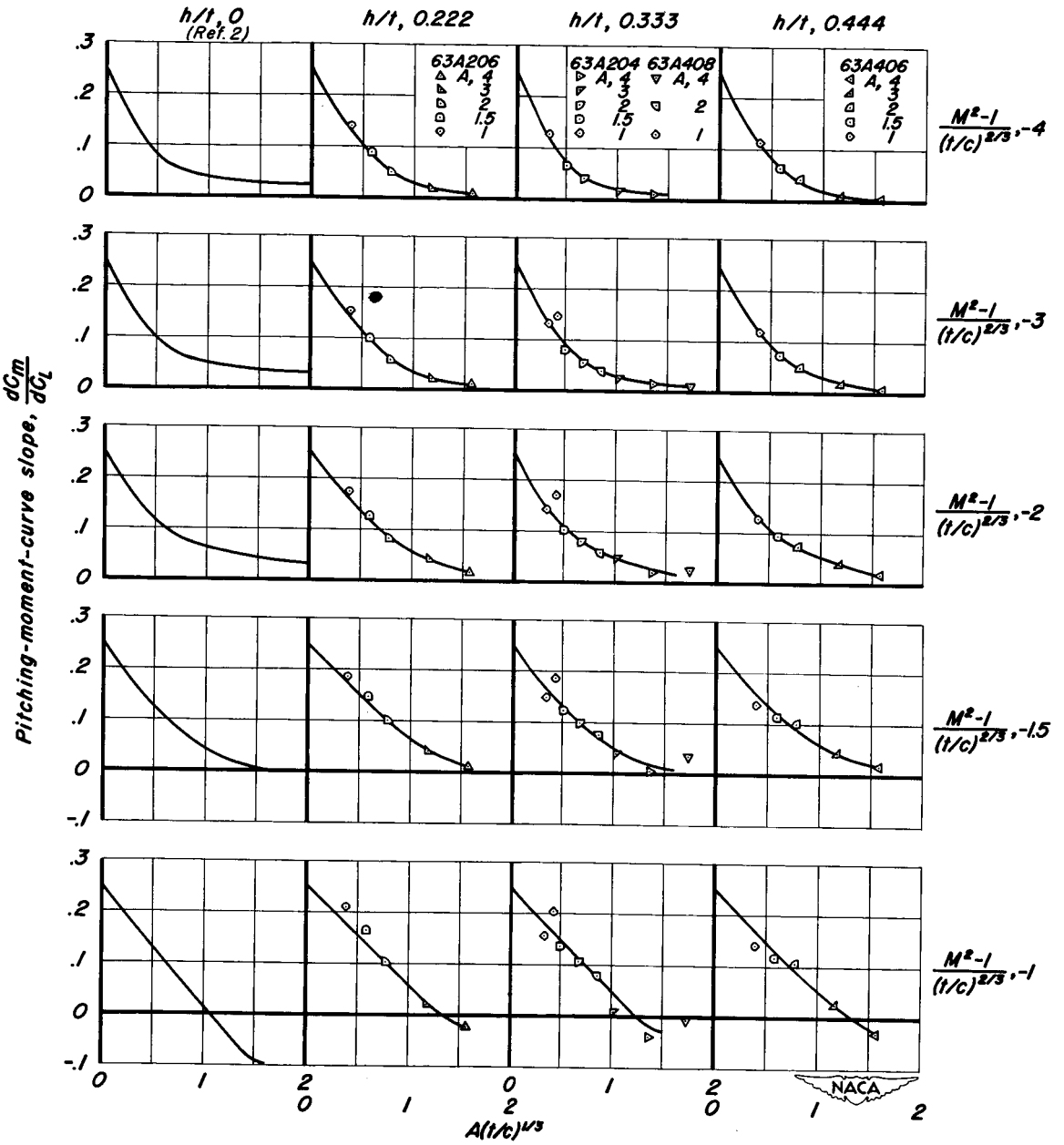

(a) $\frac{M^2-1}{(t/c)^{2/3}}$, -4, -3, -2, -1.5, and -1

Figure 24.- Correlation of pitching-moment-curve slope. $\frac{a}{(t/c)} = 0$.

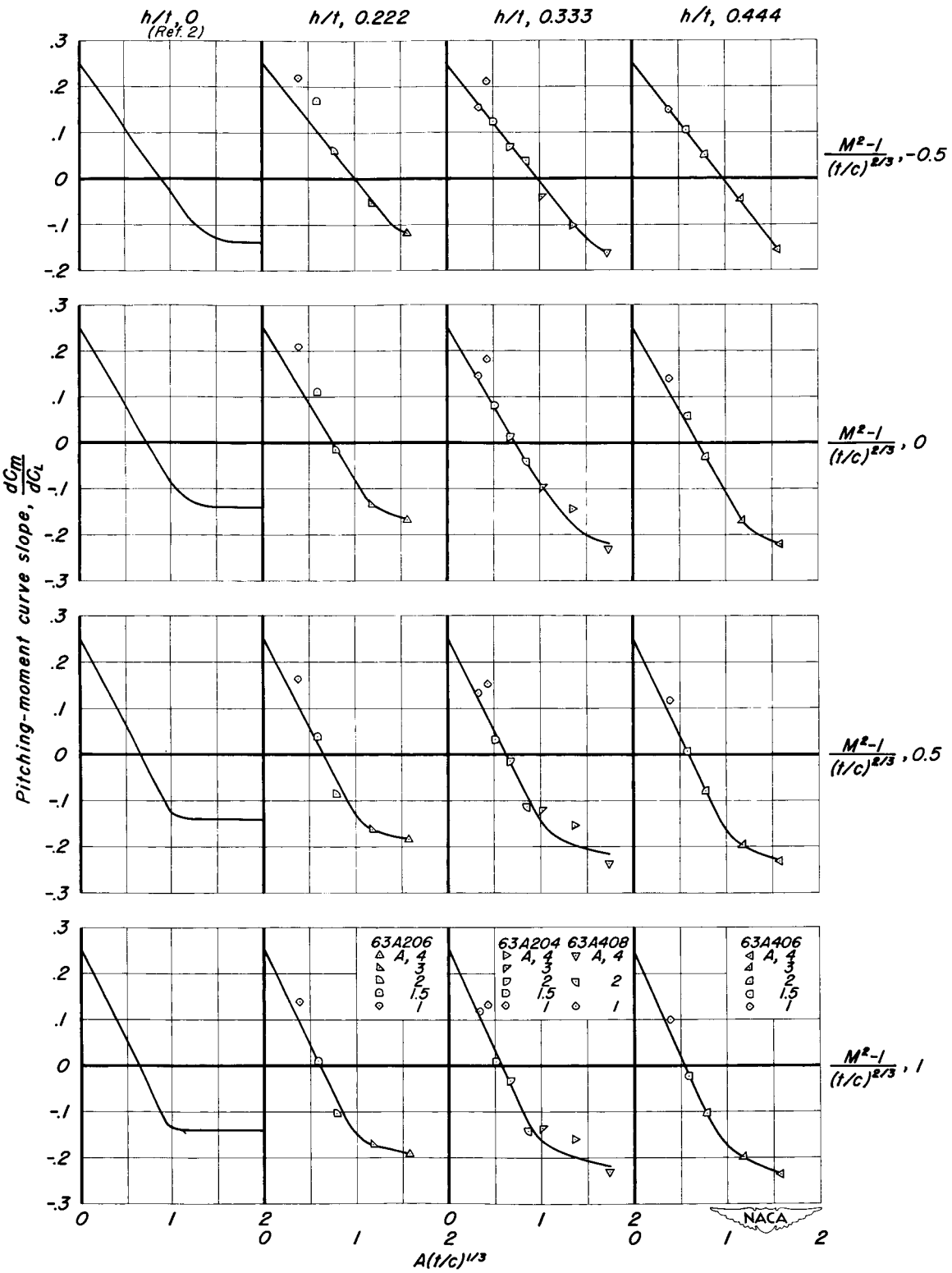

(b) $\frac{M^2-1}{(t/c)^{2/3}}$, -0.5, 0, 0.5, and 1

Figure 24.– Concluded.

[redacted]

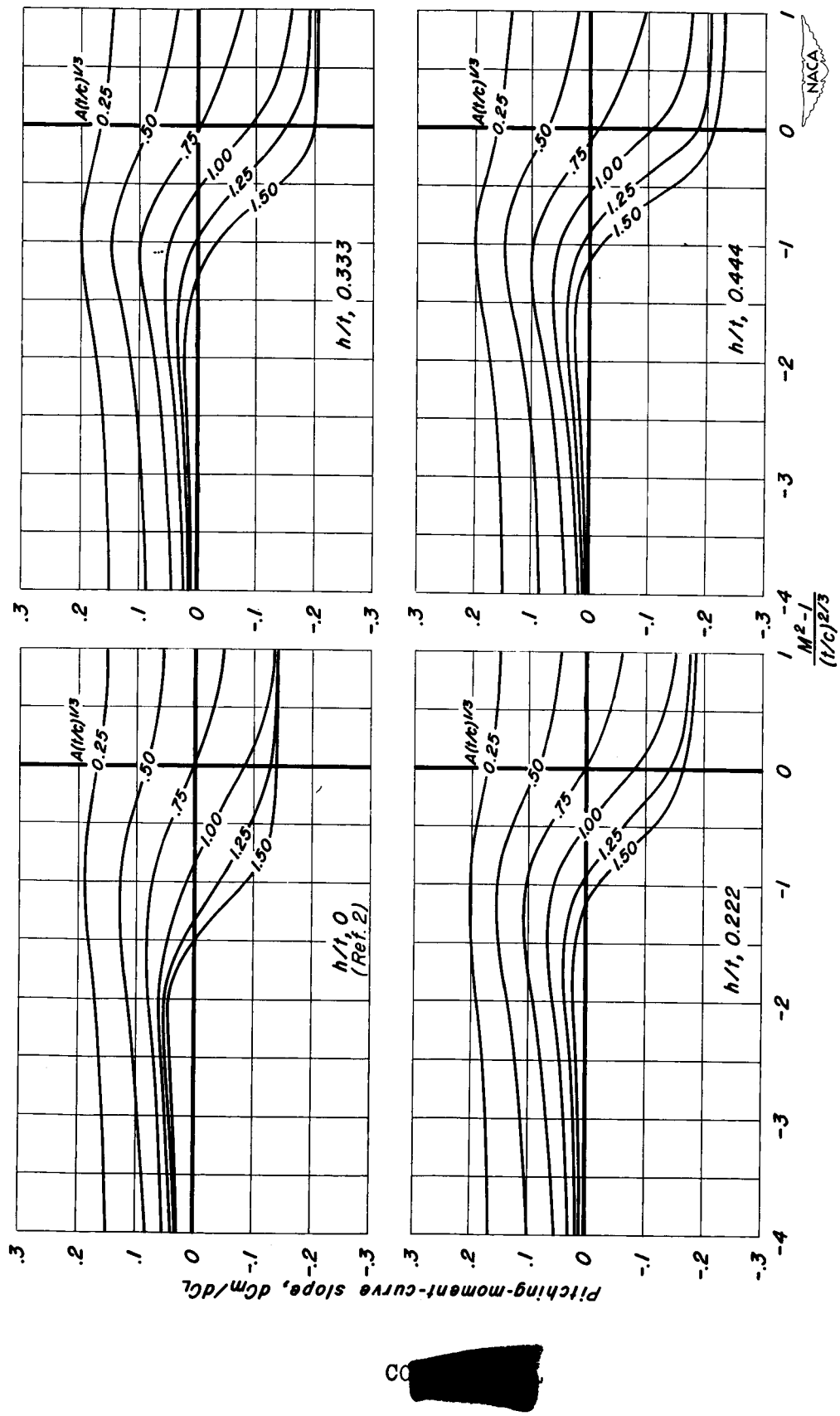

Figure 25.–Cross plot of the faired curves for pitching-moment-curve slope for NACA 63AXXX airfoils with a=0.8 mean line.

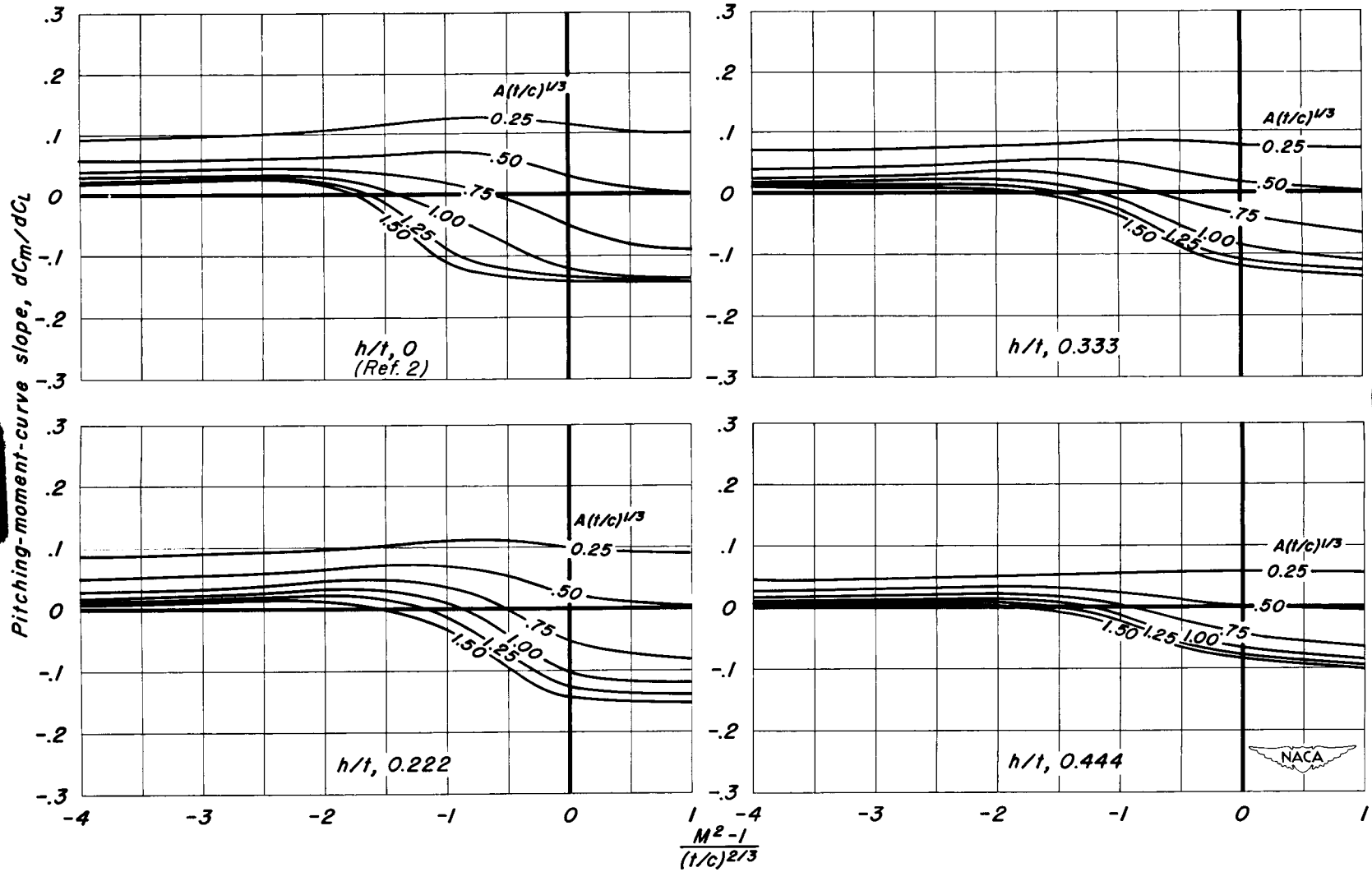

(b), $\frac{a}{(t/c)} = 1$

Figure 25.- Continued.

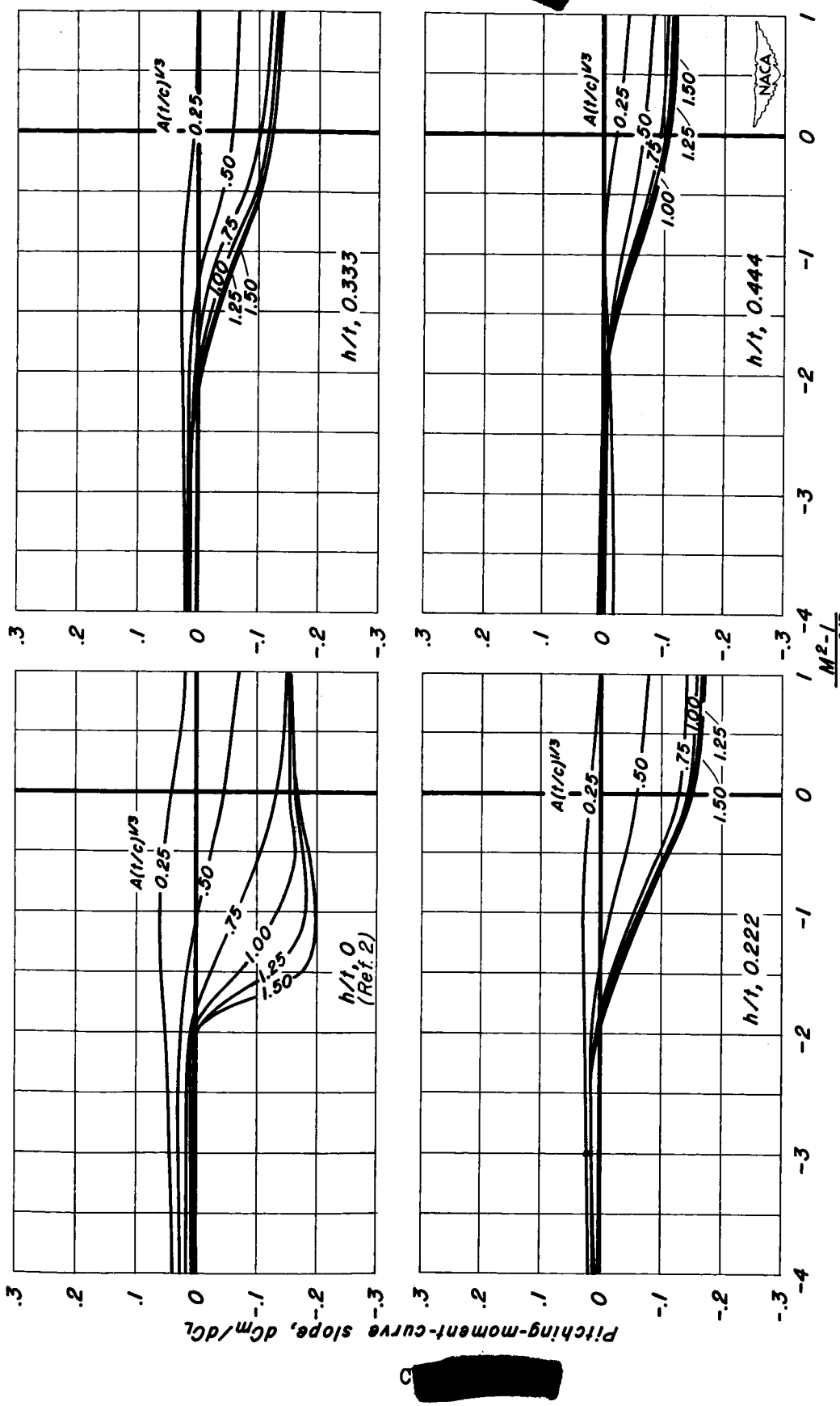

Figure 25.- Concluded.

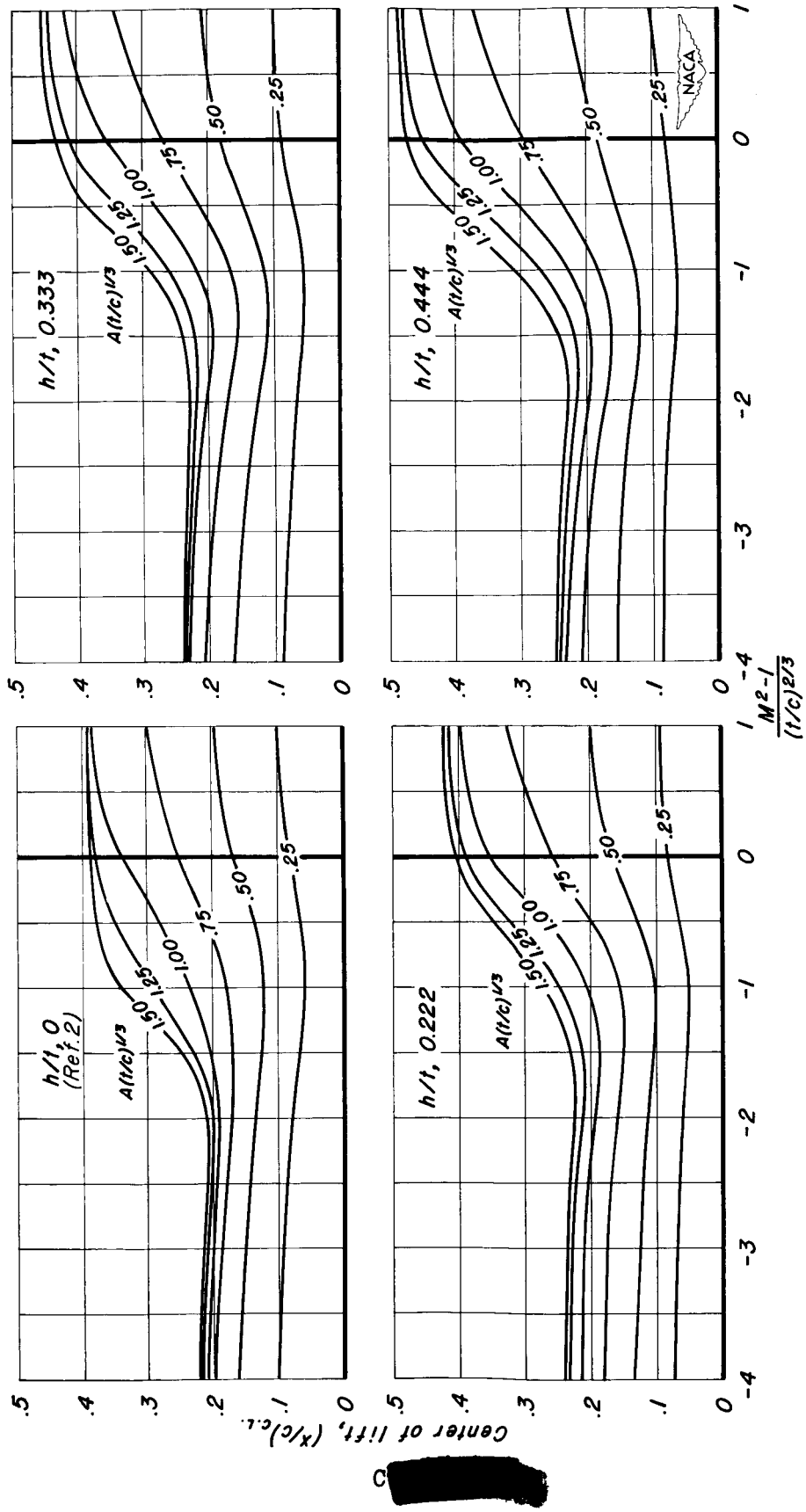

Figure 26.-Cross plot of the faired curves for the center-of-lift travel for NACA 63AXXX airfoils with a=0.8 mean line.

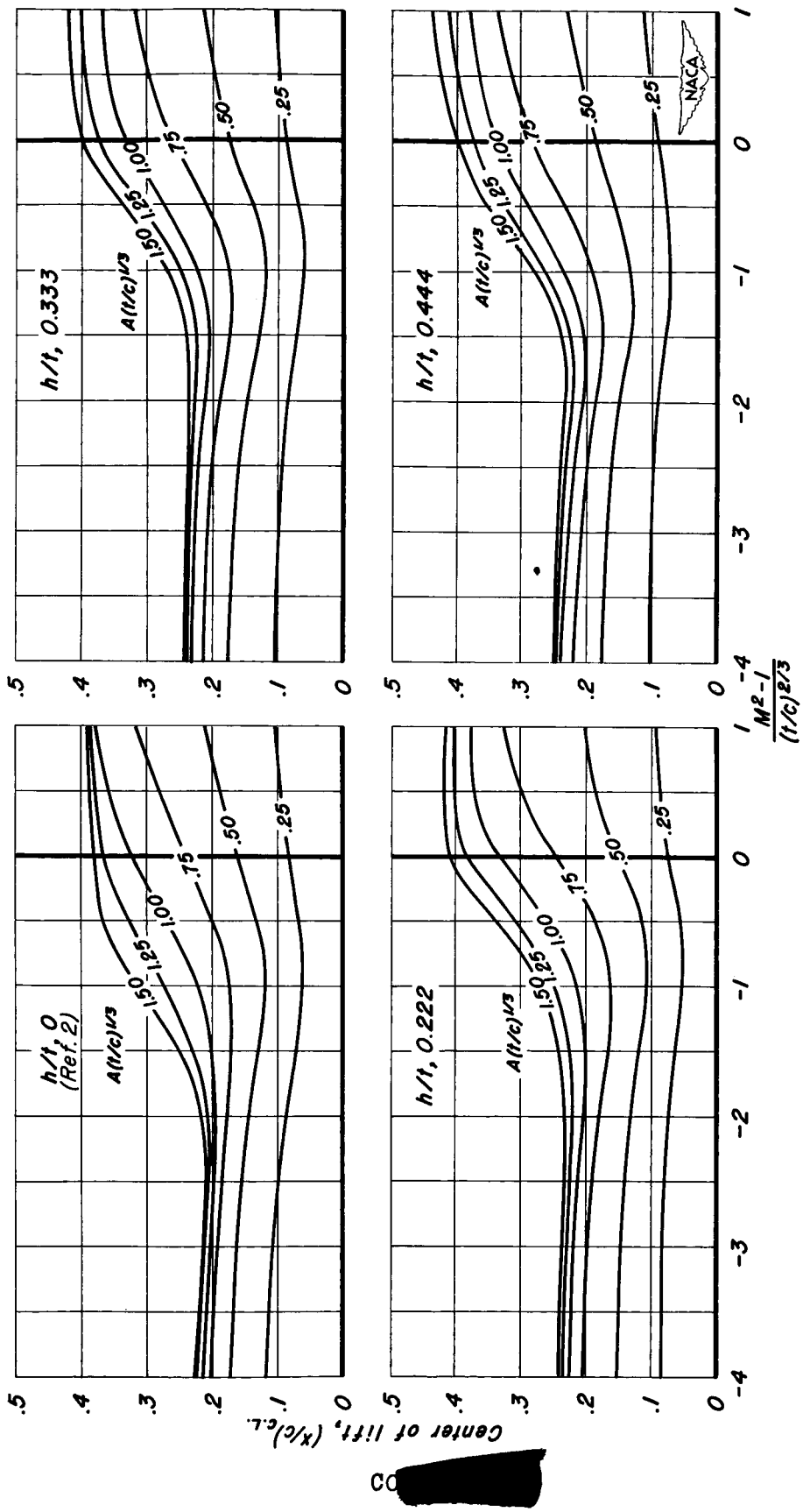

Figure 26.–Continued.

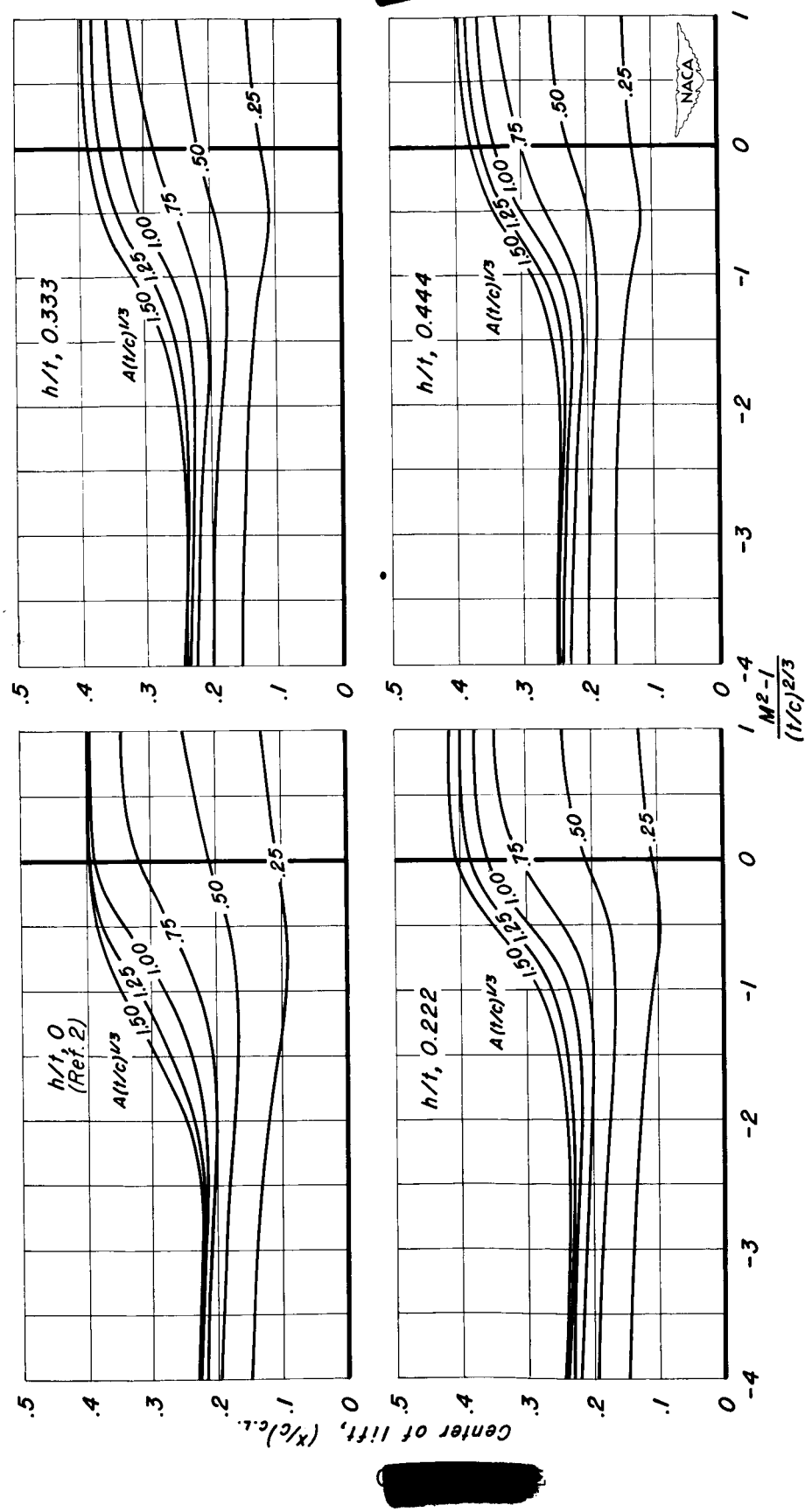

(c) $\frac{a}{t/c}$, 2

Figure 26.–Concluded.

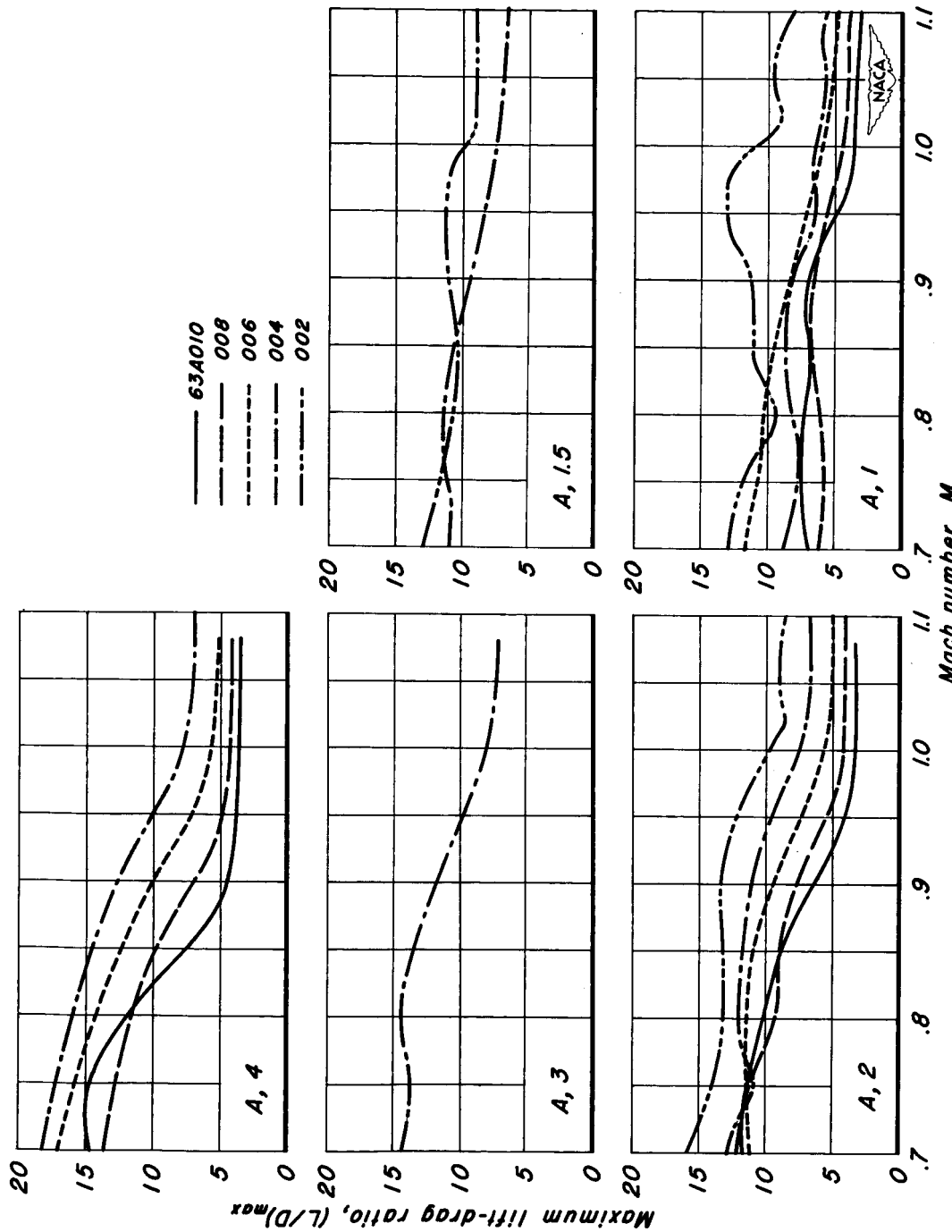

Figure 27.- The variation of maximum lift-drag ratio with Mach number.
(a) NACA 63AOXX sections.

C[redacted]

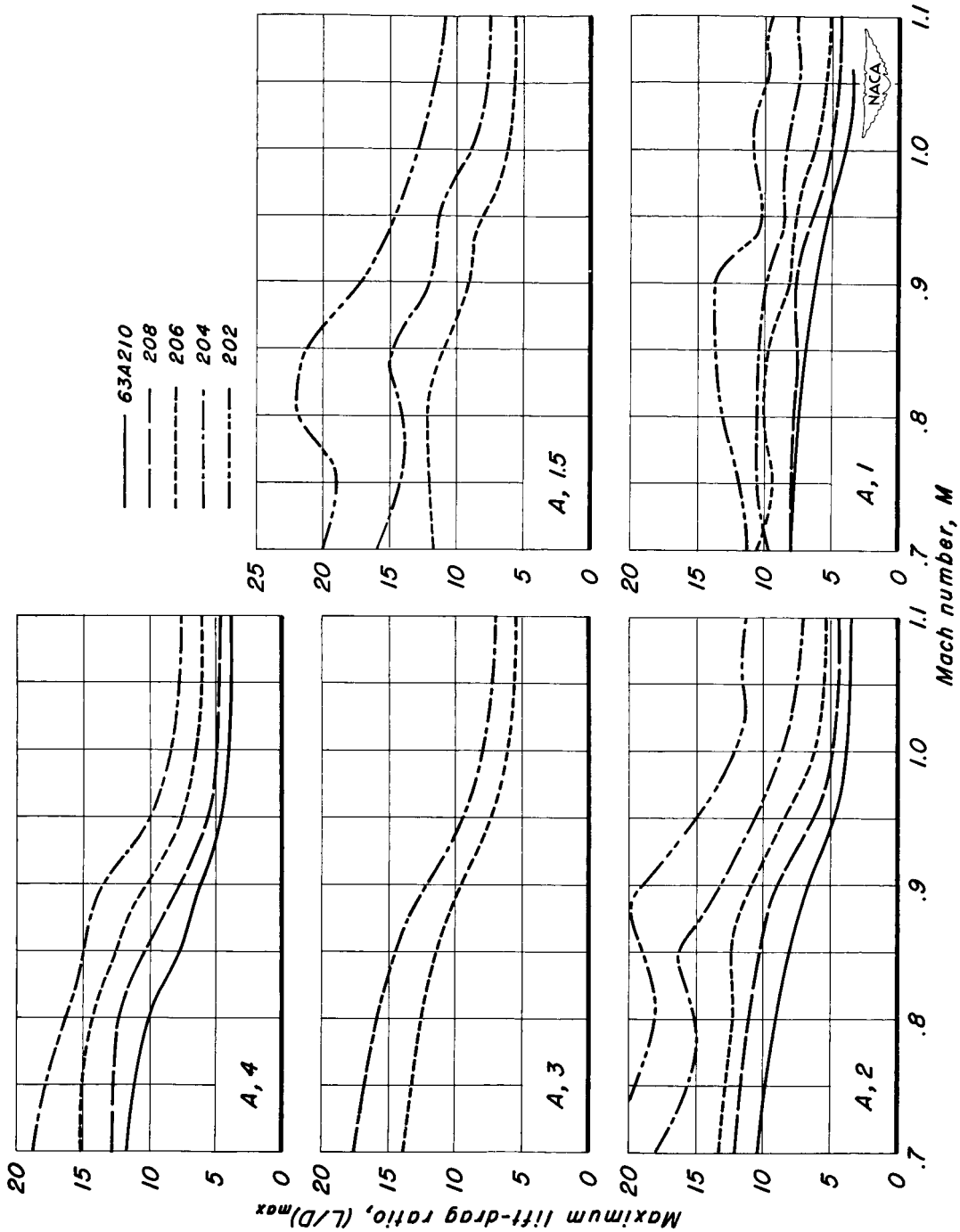

(b) NACA 63A2XX sections.
Figure 27.- Continued.

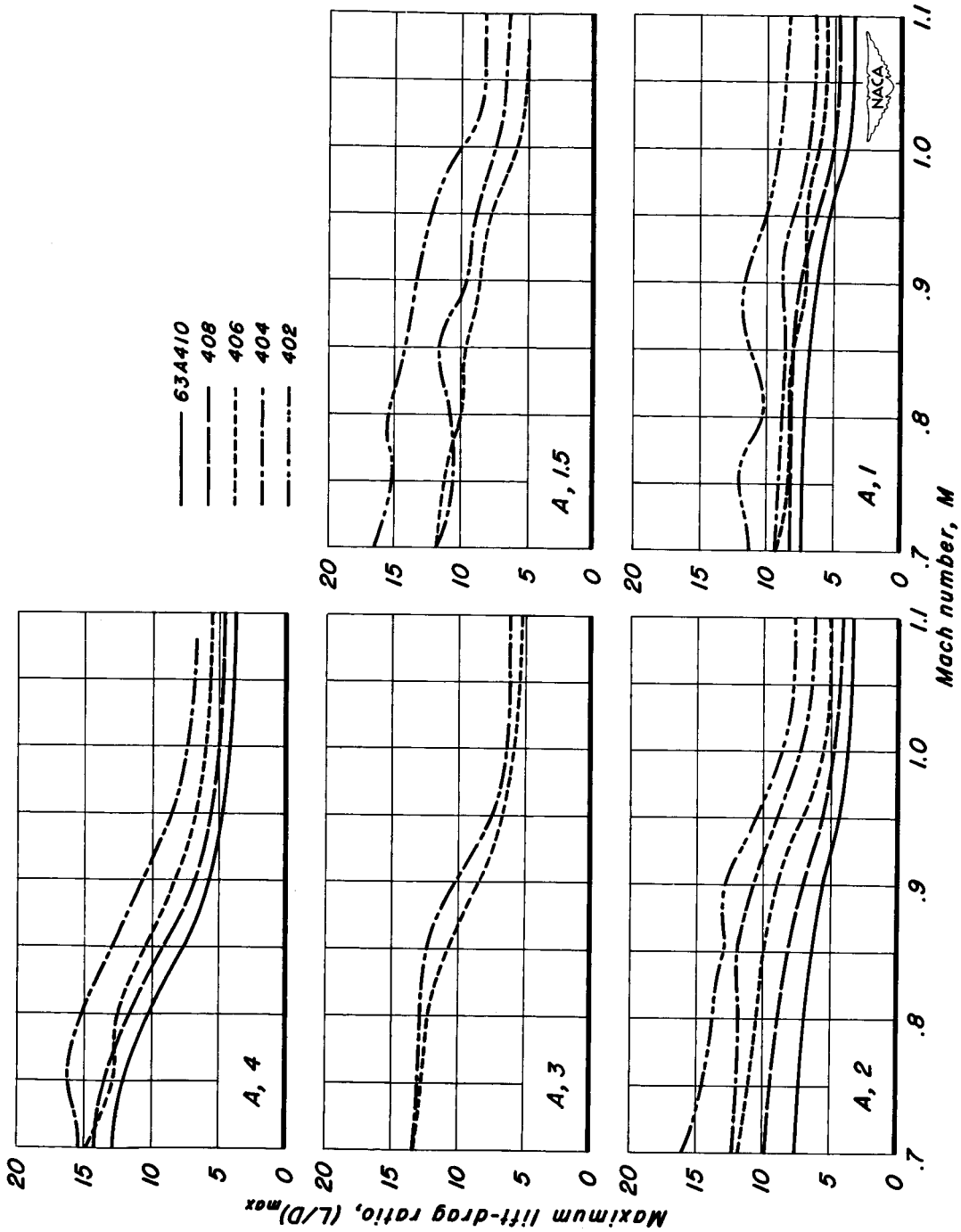

(c) NACA 63A4XX sections
Figure 27.- Concluded.

[redacted]

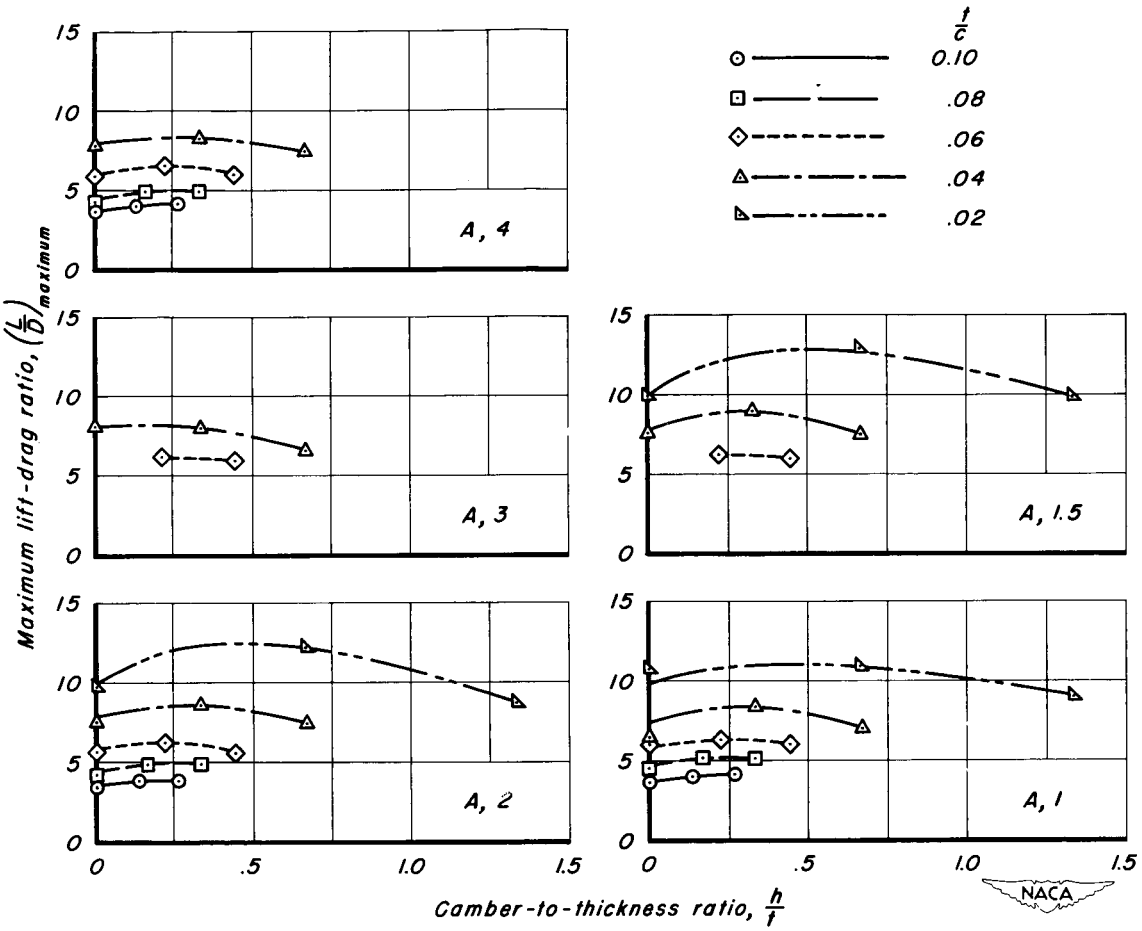

Figure 28.–The variation of maximum lift-drag ratio with camber-to-thickness ratio at M = 1.

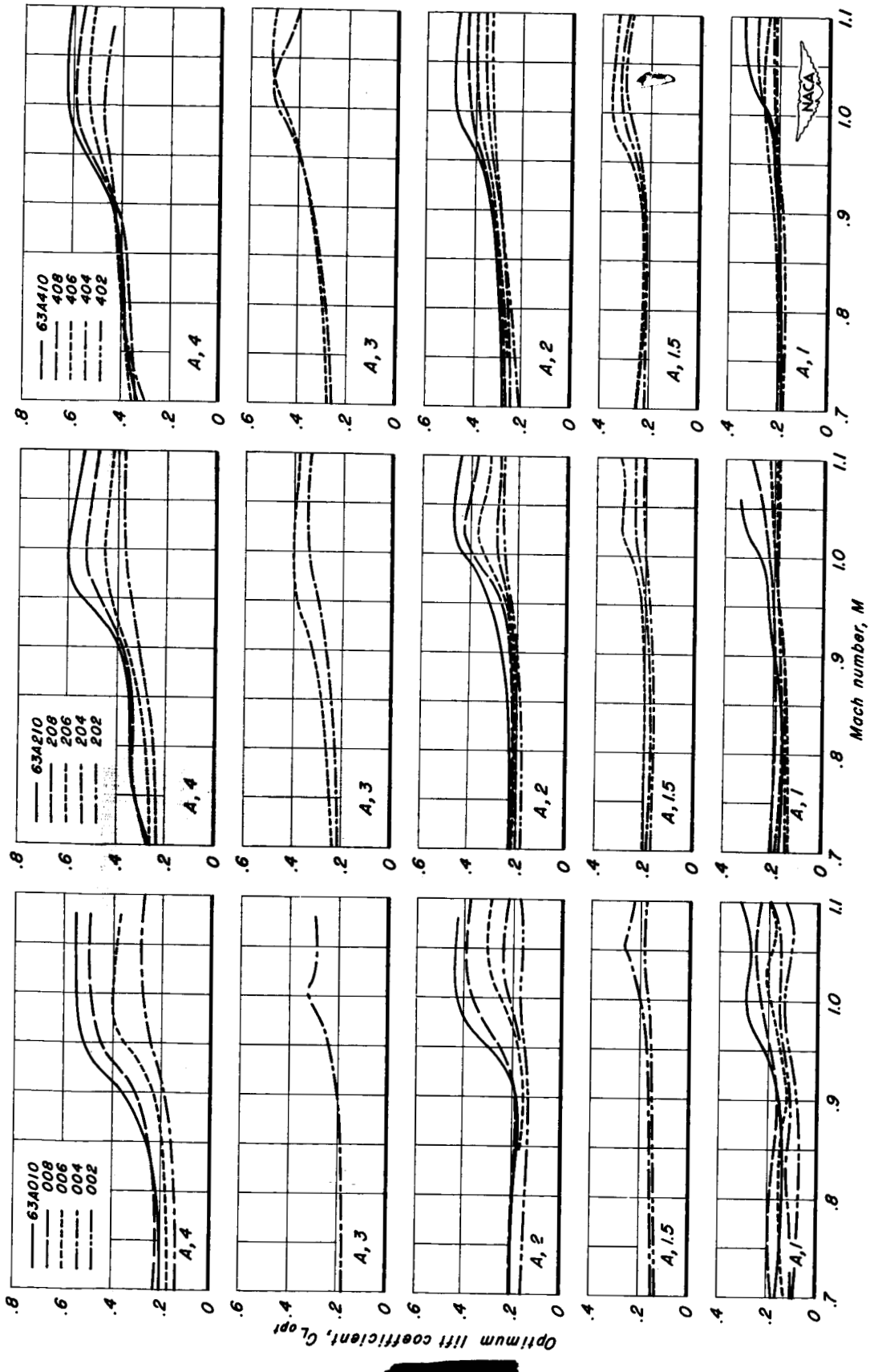

Figure 29.–The variation of lift coefficient for maximum lift-drag ratio with Mach number.